The Astrophysical Journal, 693:617–633, 2009 March 1 doi:10.1088/0004-637X/693/1/617

THE ELLIPTICITIES OF CLUSTER EARLY-TYPE GALAXIES FROM $z \sim 1$ TO $z \sim 0$: NO EVOLUTION IN THE OVERALL DISTRIBUTION OF BULGE-TO-DISK RATIOS*

B. P. Holden[1], M. Franx[2], G. D. Illingworth[1], M. Postman[3], A. van der Wel[4], D. D. Kelson[5], J. P. Blakeslee[6], H. Ford[4], R. Demarco[4], and S. Mei[4,7,8]

[1] UCO/Lick Observatories, University of California, Santa Cruz 95065, USA; holden@ucolick.org; gdi@ucolick.org
[2] Leiden Observatory, P.O. Box 9513, 2300 RA, Leiden, The Netherlands; franx@strw.leidenuniv.nl
[3] Space Telescope Science Institute, Baltimore, MD 21218, USA; postman@stsci.edu
[4] Department of Physics & Astronomy, Johns Hopkins University, Baltimore, MD 21218, USA; wel@pha.jhu.edu; ford@pha.jhu.edu; demarco@pha.jhu.edu
[5] Observatories of the Carnegie Institution of Washington, Pasadena, CA 91101, USA; kelson@ociw.edu
[6] Herzberg Institute of Astrophysics, National Research Council of Canada, Victoria, BC V9E2E7, Canada; john.blakeslee@nrc.ca
[7] University of Paris Denis Diderot, 75205 Paris Cedex 13, France
[8] GEPI, Observatoire de Paris, Section de Meudon, 5 Place J. Janssen, 92195 Meudon Cedex, France; simona.mei@obspm.fr

Received 2008 August 22; accepted 2008 November 10; published 2009 March 2

ABSTRACT

We have compiled a sample of early-type cluster galaxies from $0 < z < 1.3$ and measured the evolution of their ellipticity distributions. Our sample contains 487 galaxies in 17 $z > 0.3$ clusters with high-quality space-based imaging and a comparable sample of 210 galaxies in 10 clusters at $z < 0.05$. We select early-type galaxies (elliptical and S0 galaxies) that fall within the cluster R_{200}, and which lie on the red-sequence in the magnitude range $-19.3 > M_B > -21$, after correcting for luminosity evolution as measured by the fundamental plane. Our ellipticity measurements are made in a consistent manner over our whole sample. We perform extensive simulations to quantify the systematic and statistical errors, and find that it is crucial to use point-spread function (PSF)-corrected model fits; determinations of the ellipticity from *Hubble Space Telescope* image data that do not account for the PSF "blurring" are systematically and significantly biased to rounder ellipticities at redshifts $z > 0.3$. We find that neither the median ellipticity, nor the shape of the ellipticity distribution of cluster early-type galaxies evolves with redshift from $z \sim 0$ to $z > 1$ (i.e., over the last ~ 8 Gyr). The median ellipticity at $z > 0.3$ is statistically identical with that at $z < 0.05$, being higher by only 0.01 ± 0.02 or $3 \pm 6\%$, while the distribution of ellipticities at $z > 0.3$ agrees with the shape of the $z < 0.05$ distribution at the 1–2% level (i.e., the probability that they are drawn from the same distribution is 98–99%). These results are strongly suggestive of an unchanging overall bulge-to-disk ratio distribution for cluster early-type galaxies over the last ~ 8 Gyr from $z \sim 1$ to $z \sim 0$. This result contrasts with that from visual classifications which show that the fraction of morphologically-selected disk-dominated early-type galaxies, or S0s, is significantly lower at $z > 0.4$ than at $z \sim 0$. We find that the median disk-dominated early-type, or S0, galaxy has a somewhat higher ellipticity at $z > 0.3$, suggesting that rounder S0s are being assigned as ellipticals. Taking the ellipticity measurements and assuming, as in all previous studies, that the intrinsic ellipticity distribution of both elliptical and S0 galaxies remains constant, then we conclude from the lack of evolution in the observed early-type ellipticity distribution that the relative fractions of ellipticals and S0s do not evolve from $z \sim 1$ to $z = 0$ for a red-sequence selected samples of galaxies in the cores of clusters of galaxies.

Key words: galaxies: clusters: general – galaxies: clusters: individual (CL 1226.9+3332) – galaxies: elliptical and lenticular, cD – galaxies: evolution – galaxies: fundamental parameters – galaxies: photometry

Online-only material: color figures

1. INTRODUCTION

S0 galaxies are enigmatic objects whose formation and evolution is still not well understood. Originally, these galaxies were postulated to exist as a transition class between the elliptical and spiral sequence (Hubble 1936). Both elliptical and S0 galaxies lack spiral arms or major dust features. However, early work on the ellipticity distributions of galaxies showed that S0 galaxies were disk-dominated systems with ellipticity distributions that differed from ellipticals, being more similar to spiral galaxies in their intrinsic shapes (e.g., Rood & Baum 1967; Sandage et al. 1970). The early work on the morphology–density relation by Dressler (1980a) emphasized that S0s and ellipticals both occur with higher frequency in higher density environments, while the pioneering studies of Butcher & Oemler (1984) and Dressler & Gunn (1992) began to provide hints about how the early-type population of elliptical and S0 galaxies might evolve out to redshifts around 0.5 and earlier.

However, it was not until *HST* allowed comprehensive high-resolution imaging of distant clusters of galaxies that Dressler et al. (1997), for example, and others began to show directly that the S0 fraction was changing at high redshift. This early work, along with more recent studies (e.g., Postman et al. 2005; Desai et al. 2007) found smaller S0 galaxy fractions in clusters of galaxies at higher redshifts, $z > 0.3$–0.4. The implication is that the S0 galaxy population forms with different time-scales and later than the elliptical population. Fasano et al. (2000), Smith

* Based on observations with the NASA/ESA *Hubble Space Telescope*, obtained at the Space Telescope Science Institute, which is operated by the Association of Universities for Research in Astronomy, Inc. under NASA contract No. NAS5-26555. Some of the data presented herein were obtained at the W.M. Keck Observatory, which is operated as a scientific partnership among the California Institute of Technology, the University of California and the National Aeronautics and Space Administration. The Observatory was made possible by the generous financial support of the W.M. Keck Foundation. This paper includes data gathered with the 6.5 m Magellan Telescopes located at Las Campanas Observatory, Chile.

et al. (2005), Postman et al. (2005), Poggianti et al. (2006), Desai et al. (2007) and, most recently, Wilman et al. (2009) all find that the majority of evolution occurs since $z \sim 0.4$, i.e., in the past 4 Gyrs, and above those redshifts there is little or no evolution in the early-type galaxy fraction in clusters of galaxies out to $z \sim 1$ (see Smith et al. 2005, for a different point of view). Since S0 and elliptical galaxies have different ellipticity distributions and bulge-to-disk distributions, two simple (and related) predictions that can be drawn from the observed changes in S0 fraction with redshift is that both the mean bulge-to-disk ratio of early-type cluster galaxies and the ellipticity distribution should have changed over relatively recent epochs (since $z \sim 0.4$).

The evidence for evolution in the S0 population of clusters rests primarily on morphological classifications of galaxies. The separation of the early-type galaxy population into S0 and elliptical galaxies has long been recognized as being a challenging task (see, for example, Andreon 1998 for a discussion of the systematic errors in classification and how misclassification mimics evolution). S0 galaxies are defined as multicomponent disk galaxies, while ellipticals are defined as single component systems. However, a number of quantitative studies found that a substantial fraction of ellipticals have "disky" isophotes (see Kormendy & Djorgovski 1989, for a summary) in contrast with this definition. The analysis of Rix & White (1990) exemplifies the challenge of establishing the relative contributions of elliptical and S0 galaxies. They showed, for a $z \sim 0$ galaxy, that detecting a disk component in a spheroidal galaxy is increasingly difficult as the disk becomes more face-on in projection. Rix & White (1990) found that a disk containing 20% of the total light of a galaxy is impossible to detect over half of the range of $\cos(i)$ where i is the inclination angle. Specifically, they note "since the cos i axis can be interpreted as a probability axis, this implies that 50% of all disk with $L_D/L_B < 0.25$ cannot be detected by photometric means." These, however, results are for a single galaxy. For an ensemble of galaxies, the bulge-to-disk ratio distribution can be constrained by the intrinsic ellipticity distribution, with the average observed ellipticity being directly related to the intrinsic ellipticity (Binney & Merrifield 1998). Therefore, examining the distribution of galaxy ellipticities provides a direct measure of the evolution in the distribution of the bulge-to-disk ratios of that galaxy population.

Jørgensen & Franx (1994) investigated the ellipticity distribution of elliptical and S0 galaxies in the Coma cluster, and suggested that elliptical and S0 galaxies were not distinct classes but were part of a continuum of objects of varying bulge-to-disk ratios. This result was given additional support by a recent study by Krajnovic et al. (2008) who found that 69% of elliptical galaxies have multiple kinematic components, generally disk-like components, while 92% of S0 galaxies have disk-like components. These results give emphasis to the view that elliptical and S0 galaxies form a continuum distribution of disk fraction as opposed to two distinct classes. In particular, Jørgensen & Franx (1994) constructed a model of the ellipticity distribution of elliptical and S0 galaxies using a continuum of bulge and disk components viewed from a variety of angles. Jørgensen & Franx (1994) found a deficit of round S0 galaxies, in contrast with what was expected from their model, suggesting that some face-on S0 galaxies had been classified as ellipticals. Blakeslee et al. (2006) and Mei et al. (2006a) also found a lack of round S0 galaxies in three $z \sim 1$ clusters of galaxies when compared to what was expected for a disk population viewed at a variety of angles. These three studies illustrate a potential bias in the visual classification of galaxies, namely that nearly face-on S0 galaxies galaxies may be incorrectly classified as ellipticals. A number of studies suggest that quantitative measurements do not suffer the same orientation bias as visual classifications (Blakeslee et al. 2006; van der Wel & van der Marel 2008), but robust, bias-free galaxy classification, either visual or quantitative, still remains an elusive goal.

The importance of the work showing an apparent evolution in the S0 fraction in clusters and the knowledge of potential classification biases led Dressler et al. (1997) and Postman et al. (2005) to investigate the ellipticity distributions of the S0 and elliptical galaxies in their samples. In general, the authors found that the ellipticity distributions of S0 and elliptical galaxies show no evolution over the broad redshift ranges in their samples (Postman et al. 2005, compared clusters from $z \sim 0.25$ to $z \sim 1.3$). Also, the ellipticity distributions of elliptical and S0 galaxies differ from each other, providing evidence for the existence of two distinct classes of galaxies. However, these previous studies do not use a consistent measure of the ellipticity as compared with the $z \sim 0$ efforts such as Jørgensen & Franx (1994) or Andreon et al. (1996), making a comparison between these $z > 0.2$ samples observed with *HST* and $z \sim 0$ samples observed from the ground difficult. Traditionally, ellipticities for galaxies at $z \sim 0$ were measured by visual estimates (Dressler 1980a) or by fitting models to the elliptical isophotes (Jørgensen & Franx 1994; Andreon et al. 1996). At higher redshifts, $z > 0.2$, the ellipticities in Smail et al. (1997) or Postman et al. (2005) are determined by the second-order flux-weighted moments of a detection isophote.

Both the data and the techniques have matured so that we can now evaluate the ellipticity distribution, as a function of redshift, quantitatively, and even more importantly, in a consistent way with minimal systematic error. We show that some approaches used previously that could not correct for the point-spread function (PSF) are probably subject to significant systematic error. Essentially, the "blurring" effect of the PSF will lead to galaxies being measured as rounder than they actually are. We will use a single-consistent and robust approach for measuring the ellipticities at all redshifts. The ellipticities will be measured by fitting models convolved with the PSF to galaxy surface brightness profiles. This will eliminate some of the previously-reported uncertainties found when comparing ground-based imaging data taken under different seeing conditions (see Andreon et al. 1996, for some discussion). In addition, this approach essentially eliminates the systematic error associated with the PSF "blurring." Our ellipticity measurements will provide an assessment of the evolution in the distribution of the overall bulge-to-disk ratio of early-type cluster galaxies from the present day to redshifts $z \sim 1$.

We will discuss how we compiled our samples of early-type cluster galaxies with morphological classifications in Section 2, and then how we measured their total magnitudes, colors, and ellipticities in Section 3. One of the advantages of our approach of using an automated measurement technique is that we can simulate the measurement process. We discuss this in Section 3.3 and in Appendix A1. From our measurements, we find no evolution in the distribution of ellipticities of cluster early-type galaxies, which we show in Section 4. In Section 5, we discuss the implications of this result and contrast with previous measurements of the evolution in the overall distribution of the bulge-to-disk ratio of cluster early-type galaxy population. We follow this with a summary and some discussion of the broader implications in Section 6.

Table 1
$z < 0.05$ Cluster Summary

Cluster	z[a]	σ[a] (km s^{-1})	R_{200}[b] (Mpc)	# Early Type[c]
ACO 119	0.0440	744	1.13	41
ACO 168	0.0452	524	0.80	54
ACO 194	0.0178	435	0.67	9
ACO 957	0.0440	691	1.05	32
ACO 1139	0.0383	436[d]	0.67	23
ACO 1142	0.0353	417	0.64	17
ACO 1656	0.023	1008	1.55	203
ACO 1983	0.0441	433	0.66	18
ACO 2040	0.0456	602	0.92	50
ACO 2063	0.0337	521	0.80	50
ACO 2151	0.0371	786	1.20	58

Notes.
[a] The cluster redshift and σ from Struble & Rood (1999) unless otherwise noted.
[b] R_{200} is derived from σ.
[c] The number of galaxies with E, E/S0, S0/E, S0, or S/S0 classifications.
[d] From Poggianti et al. (2006).

Throughout this paper, we assume $\Omega_m = 0.27$, $\Omega_\Lambda = 0.73$, and $H_o = 71$ km s^{-1} Mpc^{-1}. All B magnitudes we list use the Vega zeropoint ($B_{\rm Vega} = B_{AB} + 0.11$). Other magnitudes where given are AB mags.

2. SAMPLE SELECTION

To carry out our study of the ellipticities of early-type galaxies from $z \sim 1$ to the current epoch, we have assembled a sample of morphologically-selected, cluster early-type galaxies ranging in redshifts from $z \sim 0$ to 1.27. The clusters used are tabulated below, as is the source of the morphologies for the galaxies samples (Section 2.2). The early-type galaxies are chosen to lie within the projected R_{200}, which we use to define cluster membership. The measurement for each galaxy of its color, magnitude, and its ellipticity, is described in Section 3.

2.1. Cluster Sample Selection

Our $z < 0.05$ sample is selected from Abell clusters in the Sloan Digital Sky Survey Fifth Data Release (Adelman-McCarthy et al. 2007; SDSS DR5). We summarize this sample in Table 1, where we list the Abell number (Abell et al. 1989) and the redshift of the cluster from Struble & Rood (1999). The last column lists the number of galaxies with early-type classification that are redshift-selected members and which lie within the projected R_{200} and are on the $g - r$ red sequence in the SDSS DR5 imaging.

To determine R_{200}, we will use the formula give in Carlberg et al. (1997), or

$$R_{200} = \frac{\sqrt{3}}{10}\frac{\sigma_1}{H(z)},$$

where σ_1 is the one-dimensional velocity dispersion and $H(z)$ is the Hubble constant at the redshift of observation. Desai et al. (2007) uses the relation from Finn et al. (2005), which is functionally the same, so effectively our selection radii are similar to Desai et al. (2007). We selected $2R_{200}/\pi$, instead of R_{200}, as a galaxy at R_{200} from the cluster center will be, on average, projected to appear at the distance $2R_{200}/\pi$ (see Limber & Mathews 1960, for example).

For the high redshift clusters, we required *Hubble Space Telescope* (*HST*) imaging with the Advanced Camera for Surveys (ACS) or the Wide Field Planetary Camera 2 (WFPC2) in multiple filters. We also required that the morphological classifications were done in a way consistent with the original Dressler (1980a) and Dressler (1980b) work. For the three clusters where $2R_{200}/\pi$ was larger than the field of view over which we had imaging data (generally, the clusters in the sample of Dressler et al. 1997), we simply used all available galaxies. We mark those clusters in Table 2 with the superscript (b). Below we will detail the sources for the morphological classifications and how we measured the total magnitudes, colors, and ellipticities.

We tabulate the $0.3 < z < 1.3$ clusters for which we have early-type galaxy samples in Table 2. In that table, we list the dispersions, inferred radii, and the final sample sizes. For CL J1226+33 we have compiled a new catalog of members which we will discuss in Appendix B. For RX J0849+4452, we compute a new dispersion. We use both redshifts from previous work (Stanford et al. 2001; Mei et al. 2006b) and unpublished ones we have recently collected (which we plan to publish in a future paper). There are a total of 18 galaxies in RX J0849+4452 with redshifts within R_{200}. The biweight center of the distribution is $z = 1.2600 \pm 0.0017$ and the dispersion is 798 ± 208 km s^{-1}. The errors for both the redshift and the dispersion are estimated by bootstrapping the redshift distribution.

For the clusters RX J0152−13, MS 1054−03, MS 2053−04, and CL 1358+62, we used the redshift catalogs from Holden et al. (2007). The faint magnitude limit we adopted corresponds to the completeness limits for our high redshift samples (Holden et al. 2007). For the remaining clusters, we included all galaxies that met our magnitude, color, morphology, and radial requirements, rejecting only those galaxies with redshifts outside of the clusters. This will mean that some cluster samples will be contaminated, i.e., some red-sequence early-type galaxies will not be members. The level of contamination is discussed below. Our $z > 0.3$ sample consists of 487 early-type galaxies while our $z < 0.05$ sample has 210 galaxies.

Many of the cluster red-sequence selections we use are tabulated in other studies. For those clusters studied by the ACS Instrument Definition Team, these red-sequence relations are summarized in Mei et al. (2009). For the remaining clusters, we derive the early-type red-sequence from the data. Whenever possible, we use existing redshift catalogs to determine the red-sequence of spectroscopic determined members. We then accept all galaxies that lie within the 2σ of that sequence, rejecting those galaxies that are known not to be members.

We know that there will be some contamination by field galaxies in our catalogs. To measure the level of contamination, we used at our redshift catalogs for MS 1054−03 and RX J0152−13 along with the catalogs of EDisCS from Halliday et al. (2004). RX J0152−13 has a known group in the foreground with colors very similar to the that of the cluster (see Holden et al. 2005, for a discussion). Nonetheless, when we consider all early-type galaxies that lie on the red-sequence for MS 1054−03 and RX J0152−13, regardless of redshift, we find a $3 \pm 1\%$ contamination rate of nonmembers. When we examine the less extremely rich sample of the EDisCS, we find a contamination fraction of $10 \pm 3\%$, which is likely more representative of the typical clusters in our sample. The small size of this contamination means we need not compute a statistical background correction for the cluster red-sequence.

2.2. Morphologies

Galaxy morphologies were obtained from the literature for all the galaxies in our sample. We use the morphologies from Dressler (1980a) for the $z < 0.05$ cluster members. We removed

Table 2
Summary of $0.3 < z < 1.3$ Cluster Data

Cluster	z	R.A.	Decl.	Obs. Filters	σ (km s^{-1})	R_{200} (Mpc)	# Early-type [a]
CL 1358+62	0.328[c]	13 59 50.6	+62 59 05	V_{606} I_{814}	1027^{+51}_{-45} [c]	1.4	67
CL 0024+16	0.395	00 26 35.7	+17 09 46	r_{625} i_{775} z_{850}	650^{+50}_{-50} [b]	0.83[b]	26
CL 0016+16	0.541	00 18 33.5	+16 26 14	i_{775} z_{850}	1234^{+128}_{-128} [d]	1.46[b]	42
ECL J1232−12	0.541[e]	12 32 30.3	−12 50 36	V I, I_{814}	1080^{+119}_{-99} [e]	1.28	21
CL 0054−27	0.56	00 56 56.9	−27 40 30	V_{606} I_{814}	1180[f]	1.38[b]	19
MS 2053−04	0.587	20 56 21.3	−04 37 51	V_{606} I_{814}	865^{+71}_{-71} [g]	1.00	31
ECL J1054−11	0.697[e]	10 54 24.4	−11 46 19	V I, I_{814}	589^{+78}_{-70} [e]	0.64	5
ECL J1040−11	0.704[e]	10 40 40.3	−11 56 04	V I, I_{814}	418^{+55}_{-45} [e]	0.45	2
ECL J1054−12	0.750[e]	10 54 43.5	−12 45 52	V I, I_{814}	504^{+113}_{-65} [e]	0.53	13
ECL J1216−12	0.794[e]	12 16 45.3	−12 01 18	V I, I_{814}	1080^{+119}_{-89} [e]	1.04	31
MS 1054−03	0.831[h]	10 57 00.0	−03 37 36	V_{606} i_{775} z_{850}	1156^{+82}_{-82} [h]	1.16	59
RX J0152−13	0.834[i]	01 52 43.8	−13 57 19	r_{625} i_{775} z_{850}	919^{+168}_{-168} [j]	0.92	36
CL J1226+33	0.890	12 26 58.2	+33 32 49	V_{606} I_{814}	1143^{+162}_{-162}	1.11	46
CL 1604+4304	0.897[k]	16 04 24.0	+43 04 38	V_{606} I_{814}	962^{+141}_{-141} [k]	0.93	26
CL 1604+4321	0.924[k]	16 04 33.6	+43 21 04	V_{606} I_{814}	640^{+71}_{-71} [k]	0.61	15
RX J0910+5422	1.106[l]	09 10 44.9	54 22 08.9	i_{775} z_{850}	675^{+190}_{-190} [l]	0.58	12
RX J1252−2927	1.237[m]	12 52 48	−29 27 00	i_{775} z_{850}	747^{+74}_{-84} [m]	0.60	16
RX J0849+4452	1.260	08 48 58.66	44 51 57.0	i_{775} z_{850}	798^{+208}_{-208}	0.63	8

Notes.
[a] The number of galaxies classified as early types with $-19.3 > M_B - 1.208z > -21$.
[b] Imaging area smaller than $2R_{200}/\pi$.
[c] Fisher et al. (1998).
[d] Carlberg et al. (1996).
[e] Halliday et al. (2004).
[f] Dressler et al. (1999).
[g] Tran et al. (2003).
[h] Tran et al. (2007).
[i] Blakeslee et al. (2006).
[j] Demarco et al. (2005).
[k] Gal et al. (2005).
[l] Mei et al. (2006a).
[m] Demarco et al. (2007).

all late-type galaxies from that low redshift sample, i.e., all those classified as spiral, irregular, or unknown classifications. We considered galaxies classified as S0/a as S0, and galaxies classified as Sa/0 as spirals. We list in Table 1 the number of early-type galaxies—E through S0/a—in the last column. The numbers are smaller than the number available in Dressler (1980a) because not all of the galaxies in each cluster are imaged in the SDSS DR5.

For our higher redshift clusters, we used the classifications of Dressler et al. (1997) as tabulated in Smail et al. (1997), Postman et al. (2005), and Desai et al. (2007). Each cluster was imaged with either ACS or WFPC2 with morphological classifications done in a manner consistent with the previous work of Dressler (1980a). The clusters MS 1054−03, RX J0152−13, CL J1226+33, CL 1604+4304, CL 1604+4321, RX J0910+5422, RX J1252−2927, and RX J0849+4452 all come from Postman et al. (2005). The MORPHS survey clusters CL 0016+16, CL 0054−27, CL 0024+16 are part of Dressler et al. (1997) sample. Five clusters from the EDisCS survey—ECL J1040−11, ECL J1054−11, ECL J1054−12, ECL J1216−12, and ECL J1232−12—have morphologies from Desai et al. (2007). Two additional, CL 1358+62 and MS 2053−04, have morphologies in Fabricant et al. (2000) and Tran et al. (2003), respectively.

3. DATA AND MEASUREMENTS

Our sample of early-type galaxies is based on a range in luminosity, corrected for the observed passive evolution to $z \sim 1$. The derivation of the total magnitudes and colors used for our sample selection is discussed below. Taking that luminosity-selected sample, we then discuss the derivation of their ellipticities. These constitute the key observable for this work, and the implications of those ellipticity measurements are discussed in the remainder of the paper. Our final selection will consist of morphologically-selected early-type galaxies on the red-sequence within a well-defined magnitude range ($-19.3 > M_B > -21$ at $z = 0$) lying within the cluster core that is defined by R_{200}. These magnitude limits correspond to $M_B^* + 1 > M_B > M_B^* - 0.75$ and to galaxies with stellar masses roughly between $10^{10.6}\ M_\odot < M < 10^{11.2}\ M_\odot$, assuming a "diet" Salpeter initial mass function (IMF) (see Bell et al. 2003, for a discussion of the IMF and the procedure we use to estimate the stellar masses of galaxies).

3.1. Total Magnitudes and Colors

Our samples were selected based on the rest-frame B magnitude. To estimate these magnitudes, we used the total magnitude in the passband closest to the rest-frame B. We also needed a color to correct the apparent magnitude in the observed passband to a rest-frame B magnitude; how this was done is outlined below. The Sérsic model fits that we used to measure the ellipticities also were used to determine the total magnitudes and the color apertures. The total magnitude is the normalization of the Sérsic model fit. For the color aperture, we used the circularized half-light radius, $r_{\rm hlr} = a_{\rm hlr}\sqrt{q}$, where q is the ratio of the minor to major axis, or $1 - \epsilon$, and $a_{\rm hlr}$ is the half-light radius along the

major axis of the best-fitting elliptical model as determined by GALFIT. These are the same apertures used in Mei et al. (2009) (see that paper for more detail).

We adjust the magnitudes of the galaxies by $1.208z$ as measured for early-type galaxies using the fundamental plane (van Dokkum & van der Marel 2007). This compensates for the mean passive evolution of the old stellar population. Our magnitude range covers $M^* - 0.7$ to $M^* + 1$ using the M^* from Norberg et al. (2002) after converting the b_J used by Norberg et al. (2002) to the B of the Johnson–Morgan system (Buser 1978) that we use in this paper. We trim our sample at $M_B < -19.3$, as our high redshift samples become incomplete fainter than that magnitude. The brighter magnitude limit is set to be $M_B < -21$ to exclude the most luminous galaxies (whose formation and evolution may differ, as is explained later in Section 4.1). Thus our adopted magnitude range is $-19.3 > M_B - 1.208z > -21$.

Using our simulations of real galaxies that we discuss in more detail in Appendix A.2, we estimate the typical error and offset for these total magnitude measurements. We find that total magnitudes as measured with ACS have an error of $\sigma = 0.10$ mag while magnitudes measured with WFPC2 have $\sigma = 0.15$ mag. There is a small offset at most redshifts, such that we measure a magnitude brighter than the actual magnitude of the simulated galaxy. For the clusters at $0.3 < z < 0.6$, this is only 0.02 mag, while it increases to 0.06 mag at $0.6 < z < 1$ and 0.10 mag at $z > 1$. This offset is the same for galaxies regardless of size, morphological type or the value of n from the Sérsic model fit. We do not apply this offset to the measured magnitudes.

To ensure a reliable measure of the color, we applied the CLEAN algorithm (Högbom 1974) to the original images in all passbands. Using CLEAN mitigates the effects of the different-sized PSF in different passbands, see Sirianni et al. (2005) for examples involving ACS. The final "CLEANed" images were used for measuring the galaxy colors within the $r_{\rm hlr}$ given above.

3.2. Redshifted Magnitudes

We transformed the observed magnitudes into redshifted magnitudes using the same process as van Dokkum & Franx (1996), Blakeslee et al. (2006), Holden et al. (2006), and Holden et al. (2007). We calculated the magnitudes of templates in the rest-frame filters. We then redshifted the templates, and computed the magnitudes in the observed filters. For the templates, we used exponentially decaying star-formation rate models from Bruzual & Charlot (2003, BC03); the same models were used in Holden et al. (2007). These models had exponential time-scales of 0.1–5 Gyr, covering a range of ages from 0.5 Gyr to 12 Gyr and three metal abundances, 2.5 solar, 1 solar, and 0.4 solar. For the rest-frame filters, we used the B and V curves from Buser (1978), specifically the B3 curve for the B_z as tabulated by BC03. We use the same templates and procedure for all of the clusters in our sample.

3.3. Ellipticities

We measured the ellipticities for our galaxies using the results from GALFIT (Peng et al. 2002). GALFIT fits an elliptical model to the surface brightness profile. Effectively, the ellipticity measurements we use are ellipticities at the half-light radius. The model is convolved with a PSF before it is compared with the data. The advantages of the approach we have used is that the GALFIT fit procedure minimizes the effect of the smoothing from the PSF. PSF "blurring" will make galaxies appear rounder than they actually are, unless the galaxies being fitted have sizes much greater than the PSF. In Appendix A, we discuss in more detail the robustness of the ellipticity measurements.

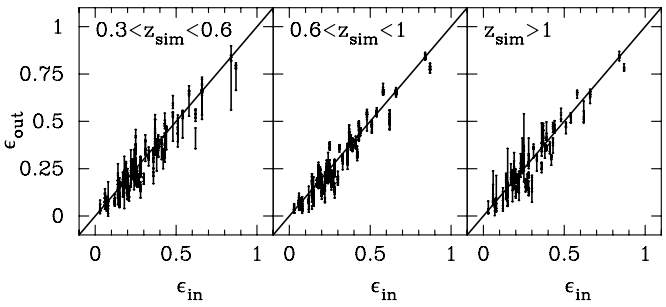

Figure 1. Ellipticity measured from the simulations, which used real galaxy images, as a function of the ellipticity in the original input image. The error bars show the scatter around the recovered ellipticity values for each galaxy. Each galaxy image is rescaled in size appropriately for the redshift of each cluster. Each galaxy is realized at a variety of signal-to-noise values covering the range over which the galaxies in the high redshift sample are observed, and were then placed in the cluster imaging data. We plot a straight line with a slope of one, the expected relation if we recover the input ellipticities. The scatter is typically $\sigma_e \sim 0.01$–0.03. The scatter increase at lower signal-to-noise, and matches the statistical errors from the fitting process. The median offset is -0.01 with a range of 0.00 to -0.03, showing that our method accurately recovers the ellipticity of these low-redshift galaxies when they are observed at high redshift. No systematic trends are seen as a function of ellipticity or redshift.

This procedure is performed for galaxies at all redshifts, but requires an estimate of the PSF. For the clusters of galaxies at $z < 0.05$, our imaging data came SDSS DR5. We use the software tools provided by the SDSS to extract the PSF appropriate for each galaxy. For the higher redshift galaxies, the pipeline processing system we use for ACS (Apsis—ACS pipeline science investigation software) provided us with suitable PSF (Blakeslee et al. 2003, 2006). We used empirical PSF models constructed from multiple ACS observations of 47 Tuc. For the WFPC2 data, the PSF still has a strong positional dependence and is significantly under sampled. For these data, we estimated the PSF using the TinyTim software package (Krist 1995) for each galaxy we fit. We also used the option in GALFIT to convolve the model of the galaxy with an over-sampled PSF. Before comparing the PSF convolved model with the data, GALFIT rebinned the model to the WFPC pixel scale and smoothed the model with the charge diffusion kernel.

3.3.1. Simulations of Ellipticity Measurements

We constructed a set of simulations using real galaxy images and placed those images in the data of the high redshift clusters in our sample. This is discussed in detail in Appendix A.2.

To summarize, we made multiple measurements of each simulated individual galaxy to assess both the impact of noise and any systematic effects, and each galaxy was simulated over a range in magnitudes. We found that the scatter in the ellipticity measurements of the images of real galaxies was $\sigma_e \sim 0.01$–0.03 at magnitudes typical of those in our samples, and only increased (to $\sigma_e \sim 0.05$–0.06) at or below the magnitude limit of our samples. These estimates of the uncertainty are in good agreement with the errors estimated by the model fitting process used to measure the ellipticity. We found no large systematic trends in the ellipticity measurements. This can be see in Figure 1 where we show the recovered ellipticity as a function of the input ellipticity for three redshift bins. There was only a very small overall shift of $\delta_e = 0.01$, or

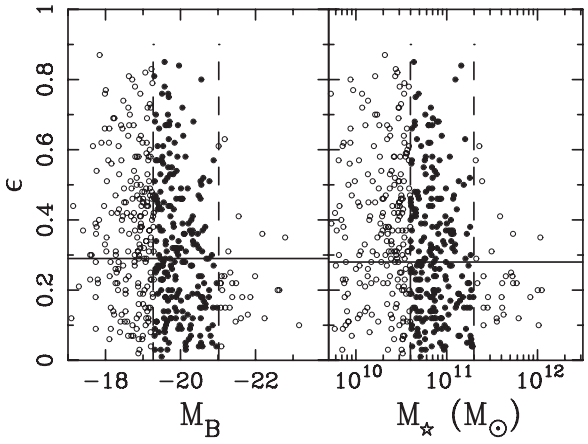

Figure 2. Ellipticity versus absolute B magnitude or stellar mass for the $z < 0.05$ clusters, as described in the text in Section 3. The dashed lines show magnitude limits we will use for this paper, $-19.3 > M_B > -21$. Below $M_B = -19.3$ our higher redshift cluster samples become incomplete, while above brighter than $M_B \sim -21$, the ellipticity distribution of the early-type galaxy population changes, becoming rounder, possibly the result of the somewhat different evolutionary history of the most massive galaxies. The galaxies within our selection limits are filled circles, while all of the remaining data are shown as open circles. The median ellipticity of the galaxies in our sample is shown by a solid line. The mass-selected sample and the luminosity-selected samples yield a very similar selection with similar median ellipticity, suggesting that mass-dependent effects are likely to be small. For the rest of the paper, we will use the B magnitude limits in the left panel to select galaxies at higher redshifts.

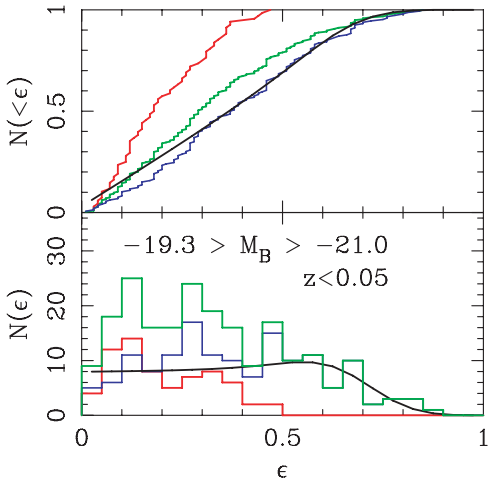

Figure 3. Ellipticity distributions for magnitude-selected samples by galaxy type for the $z < 0.05$ clusters. We show the elliptical and S0 population separately (red—ellipticals, blue—S0 galaxies, green—all early-type galaxies). The two sets of galaxies show different ellipticity distributions in our data, as expected from the results of previous work. The elliptical galaxy population shows a peaked distribution, with a median ellipticity of $\epsilon_{\rm med} = 0.18 \pm 0.01$. In contrast, the S0 galaxies have a broader ellipticity distribution, with $\epsilon_{\rm med} = 0.38 \pm 0.02$, consistent with a more disk dominated population. We show, with a black line, the best-fitting disk population drawn from a Gaussian distribution which has a mean thickness of $b = 0.27 \pm 0.10$ giving a mean ellipticity of $\bar{\epsilon} = 0.73 \pm 0.10$, with a standard deviation of $\sigma_\epsilon = 0.10 \pm 0.02$. If the S0 fraction decreases with redshift, the overall ellipticity distribution of the cluster population should also evolve as there will be fewer galaxies with large ellipticities.

(A color version of this figure is available in the online journal.)

3% for the typical galaxy, such that the typical $z > 0.3$ galaxy is measured to be slightly rounder than it would appear in the $z < 0.05$ sample. We found the shift was the same, regardless of the redshift of the galaxy. No systematic changes were seen as a function of ellipticity. For the rest of the paper, we ignore the small systematic shift of $\delta_e = 0.01$ (noted above and in Figure 1), and simply quote the observed values.

We also tested the robustness of the ellipticity measurements by using incorrect PSFs. We found that this error could result in a systematic offset of $\delta_e = \pm 0.01$ to $\delta_e = \pm 0.03$ depending on how bad the mismatch between the PSFs were. The small size of our statistical errors means that we are sensitive to systematic errors of this order, and we will discuss the implications of this in later sections.

4. ELLIPTICITY DISTRIBUTIONS

4.1. Ellipticity Distributions for the $z < 0.05$ Sample

In this section, we define our selection of $z < 0.05$ galaxies, and discuss how we will characterize the ellipticity distributions in order to compare them with the $z > 0.3$ cluster galaxy sample.

In Figure 2, we plot the ellipticity as a function of M_B, and also by stellar mass, for all galaxies in the $z < 0.05$ sample that are within $2R_{200}/\pi$, and classified as an early-type galaxy. We show the median ellipticity of the whole population with a solid line. The stellar masses are derived using the prescription from Bell et al. (2003), which uses the rest-frame colors to estimate the mass-to-light ratio of the stellar population, assuming a "diet" Salpeter IMF. The "diet" Salpeter IMF is a Salpeter IMF with truncation at very low masses, resulting in a mass-to-light ratio of the stellar population 0.15 dex smaller than a Salpeter IMF. These stellar mass estimates agree well with the mass estimates from the fundamental plane (see Holden et al. 2007).

At the highest masses or brightest magnitudes, the population becomes rounder, a result seen in other work (see Franx et al. 1991; Vincent & Ryden 2005, for example), likely a result of a different morphological mix among the most luminous galaxies which may have a somewhat different formation and evolution history. We will exclude these most luminous galaxies, $M_B < -21$, from our sample. We illustrate our sample range $-19.3 > M_B > -21$ with dashed lines in Figure 2.

At low redshifts, we know that elliptical and S0 galaxies have different ellipticity distributions. In Figure 3, we show that we reproduce those different distributions with our $z < 0.05$ cluster galaxy sample. The elliptical population, shown in red in Figure 3, is much rounder than the S0 population, shown in blue. The whole of the population is shown in green. Because S0 galaxies dominate the population, the green line appears closer to the S0 distribution than the elliptical distribution. The median ellipticities are different, with the median ellipticity of S0 galaxies $\epsilon_{\rm med} = 0.38 \pm 0.02$ while the median ellipticity of elliptical galaxies is $\epsilon_{\rm med} = 0.18 \pm 0.01$.

In Figure 3, there is a hint of a deficit of round S0 galaxies, a result found by Jørgensen & Franx (1994). We fit to the distribution of S0 ellipticities with the disk galaxy model used in Jørgensen & Franx (1994). This disk galaxy distribution is that of an oblate spheroid with the minor to major axis ratios drawn from a Gaussian distribution with mean $\bar{\epsilon}$ and a dispersion of σ_ϵ. We find that the values for the Gaussian that best describes the data are similar to that of Jørgensen & Franx (1994). Our values of $\bar{\epsilon} = 0.73 \pm 0.10$ and $\sigma_\epsilon = 0.10 \pm 0.02$ are consistent with $\bar{\epsilon} = 0.65$ and $\sigma_\epsilon = 0.10$ from Jørgensen & Franx (1994)—a difference $\sim 1\sigma$. At small ellipticity values, the ellipticity distribution of visually classified S0 galaxies fall consistently below the expectation of the model, which indicates a possible lack of round S0 galaxies.

Coma (A1656) is a dominant contributor to the early-type sample at $z < 0.05$, with about 37% of the total. We investigated

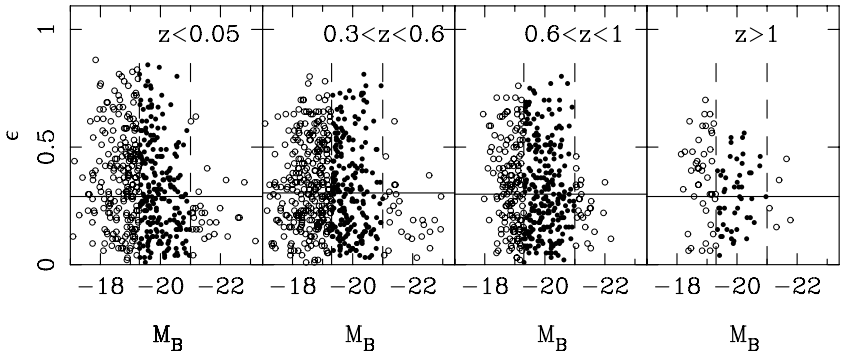

Figure 4. Ellipticity versus absolute B magnitude for all the clusters in our sample. The magnitude range, shown by the dashed lines, is the same throughout, as we derived in Figure 2. Each galaxy is selected to be within $2R_{200}/\pi$ and to have $-19.3 > M_B + 1.208z > -21$, after removing the effects of passive evolution. We assume early-type galaxies become brighter by $1.208z$ mag (van Dokkum & van der Marel 2007). In each panel, the solid dots are those in the magnitude range of our selection, while the open circles show the remaining galaxies in our sample. Each panel covers a different range in redshifts, the leftmost, $z < 0.05$, followed by $0.3 < z < 0.6$, $0.6 < z < 1.0$, and $z > 1.0$. The horizontal line is the estimate of the median ellipticity for the sample within the magnitude limits. It is striking to note that the median ellipticity distribution does not change with redshift. Only at the highest redshifts do we see a hint of fewer highly elliptical galaxies.

Table 3
Median Ellipticities of $z < 0.05$ Sample

Sample	All Early Types	S0's	Ellipticals
All $z < 0.05$ clusters	0.29 ± 0.02	0.38 ± 0.02	0.18 ± 0.01
Without Coma	0.29 ± 0.02	0.34 ± 0.03	0.21 ± 0.02

the impact of the removal of Coma from the sample. As can be seen in Table 3 doing so makes surprisingly little difference to the ellipticity measures of the early-types or of the E and S0s separately. The ellipticity is consistent within the uncertainties. The S0 fraction of the $z < 0.05$ sample is $68 \pm 3\%$ for the whole sample and $72 \pm 4\%$ without Coma.

Both Jørgensen & Franx (1994) and Andreon et al. (1996) tabulate their ellipticities. The median ellipticities in the Coma sample of Jørgensen & Franx (1994) are $\epsilon_{\rm med} = 0.34 \pm 0.02$ for the S0 galaxies and $\epsilon_{\rm med} = 0.16 \pm 0.02$ for ellipticals. Both medians are slightly rounder than our measured low redshift values, though the differences are small. The lower values are possibly due to the use of the PSF in our analysis. Jørgensen & Franx (1994) did not remove the smoothing of the PSF, and so will be offset to slightly rounder values as a result.

Andreon et al. (1996) derive ellipticities for the S0 galaxies and ellipticals. These values have been used as a low-redshift comparison set by other higher redshift studies (Smail et al. 1997; Fasano et al. 2000), it is useful to understand the difference between these measurements and ours. These ellipticities are measured at a fixed μ_R isophote and are not PSF corrected measurements at the effective radius. Thus measurement of the ellipticity from Andreon et al. (1996) is not directly comparable to ours and is not the optimal approach for our study.

4.2. $z > 0.3$ *Ellipticity Distributions*

We plot in Figure 4 the distribution of ellipticities as a function of absolute B magnitude for four redshift bins. As before, we select only those galaxies in a fixed magnitude range. We adjust the magnitudes, however, by $1.208z$ mag to reflect the amount of passive galaxy evolution that is measured from the fundamental plane (van Dokkum & van der Marel 2007). We combine each cluster's sample into three redshift bins, $0.3 < z < 0.6$, $0.6 < z < 1.0$, and $z > 1$. We show, with a solid line, the median ellipticity for the selected sample in each bin.

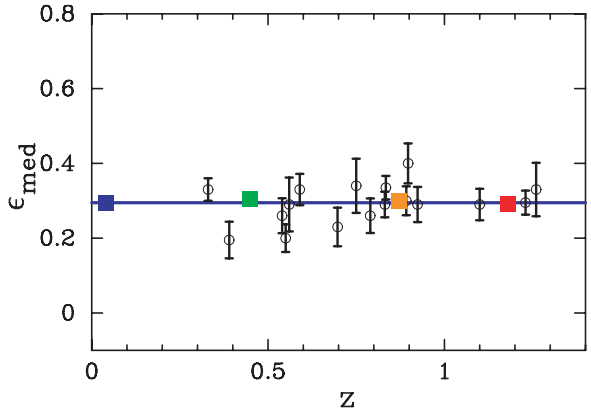

Figure 5. Median ellipticity versus redshift for the clusters in our sample. The open circles are the median ellipticities for the early-type galaxies in each cluster, after applying our magnitude and radius selection. The median ellipticity, $\epsilon_{\rm med} = 0.29 \pm 0.02$, for all of the galaxies in $z < 0.05$ cluster sample is shown by the blue square and line. The other squares are the medians for all of the cluster galaxies in the redshift ranges $0.3 < z < 0.6$ (green), $0.6 < z < 1.0$ (orange), and $z > 1$ (red) samples, respectively. The median ellipticity for the whole of the $z > 0.3$ sample is $\epsilon_{\rm med} = 0.30 \pm 0.01$. The median ellipticity for cluster galaxies in the range of $0.3 < z < 0.6$ is 0.31 ± 0.02, while the median ellipticity for cluster galaxies in the range of $0.6 < z < 1.0$ is 0.30 ± 0.02. At $z > 1$, the median ellipticity is $\epsilon_{\rm med} = 0.29 \pm 0.03$. All values are all in excellent agreement with the 0.29 ± 0.02 we find for the $z < 0.05$ sample. We find no individual clusters that have drastically different ellipticity distributions. The lack of any trend in the ellipticity, and minimal cluster-to-cluster variance, is a striking result. The median ellipticity at $z > 0.3$ is statistically identical to that at $z < 0.05$, being higher by only 0.01 ± 0.02.

(A color version of this figure is available in the online journal.)

We find no evolution in the median ellipticity with redshift. In Figure 5, we plot the median ellipticity for each cluster. In this plot, we show the median ellipticity for each cluster as open circles. For our $z < 0.05$ sample, we show just the median value (the blue square), $\epsilon_{\rm med} = 0.29 \pm 0.02$. The median values for the individual $z > 0.3$ clusters show larger scatter, but in general are quite consistent with the low redshift value, with the whole $z > 0.3$ sample having $\epsilon_{\rm med} = 0.30 \pm 0.01$. The green, orange, and red points are the median ellipticities (shown also in Figure 4 as the horizontal lines) at $0.3 < z < 0.6$ and at $0.6 < z < 1.0$ and $z > 1$, $\epsilon_{\rm med} = 0.31 \pm 0.02$, $\epsilon_{\rm med} = 0.30 \pm 0.02$, $\epsilon_{\rm med} = 0.29 \pm 0.03$, respectively. The errors we quote, here and later in the paper, are the errors on

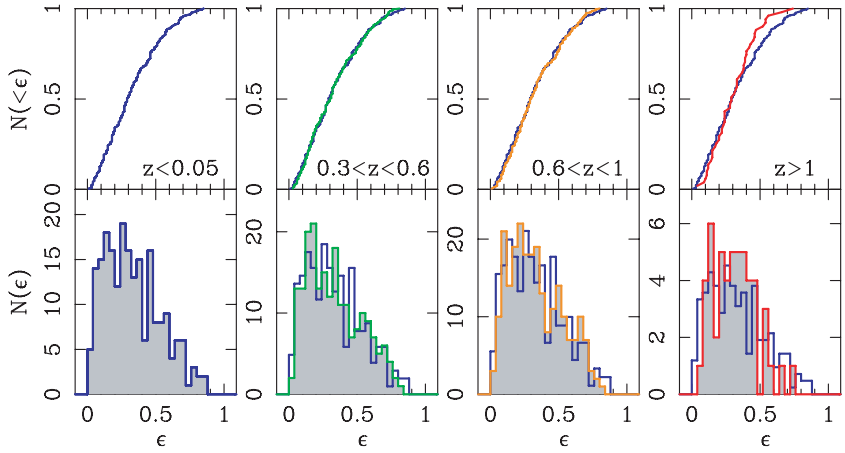

Figure 6. Cumulative (top) and differential (bottom) ellipticity distributions for our four redshift bins. In each plot, we show the distribution of the ellipticities of all early-type galaxies in our magnitude and radius selection for all of the cluster galaxies in a given redshift bin. The distributions are represented by the shaded histograms, outlined in blue for $z < 0.05$, green for $0.3 < z < 0.6$, orange for $0.6 < z < 1$, and red for $z > 1$. For comparison with the $z > 0.3$ cluster samples, we plot our sample of $z < 0.05$ early-type galaxies in blue, with the low-redshift line "hidden" when the two lines (frequently) overlap. The $z < 0.05$ sample is normalized to have the same number of galaxies as each of the $z > 0.3$ cluster samples. The small deficit of highly elliptical galaxies at $z > 1$ is not statistically significant because of the small sample size. Again, it is striking that there is no evolution in the shape of the distribution from $z < 0.05$ to $z > 1$. *The distribution of ellipticities at* $z > 0.3$ *agrees with the shape of the* $z < 0.05$ *distribution at the 1%–2% level (i.e., the probability that they are drawn from the same distribution is 98%–99%).*

(A color version of this figure is available in the online journal.)

the median, or $\sqrt{(}\pi/2)$ the error on the mean. We confirmed these error estimates with bootstrap resampling. We compared the scatter in the high redshift sample by computing the χ^2 around the low redshift median value. We find a $\chi^2_\nu = 1.27$ for $\nu = 17$ degrees of freedom, confirming both the good visual agreement between the high redshift data and that the scatter is not higher than expected from random errors. As we discuss in Appendix A.2, we expect the largest systematic errors on the median ellipticity values to be ~ 0.02, which are not large enough to shift the high redshift data to significantly smaller ellipticity values. The lack of any change in ellipticity with redshift is striking. Formally, *the median ellipticity of our sample of 487 early-type galaxies at* $z > 0.3$ *is statistically identical to that of the 210 early-type galaxies at* $z < 0.05$*, being higher by only 0.01* $\pm$ *0.02 or 3* $\pm$ *6%.*

To add a more detailed assessment of the changes and to provide a more quantitative basis for the results seen above, we plot the ellipticity distributions of the samples in Figure 6, both differentially and in cumulative form. In each figure, the blue line shows the $z < 0.05$ comparison sample, with the normalization rescaled to match the higher redshift samples. At no redshift do we find a statistically significant change in the ellipticity distribution. We use a number of tests to quantify this, including a Kolmogorov–Smirnov, Wilcoxon–Mann–Whitney rank sum test and a Kuiper test. Taking the results from these tests we find that *the distribution of ellipticities at* $z > 0.3$ *agrees with the shape of the* $z < 0.05$ *distribution at the 1%–2% level (i.e., the probability that they are drawn from the same distribution is 98%–99%).* This is a remarkable demonstration of the consistency of the ellipticity distributions over a time span of more than half the age of the universe.

There is a hint, in our $z > 1$ sample, of a lack of high ellipticity galaxies, though it is not significant in any of our tests. This is, in large part, because of the small sample size. There are only 48 galaxies in the $z > 1$ cluster sample. In Section 4.1, we showed that the median ellipticity for the $z < 0.05$ sample was essentially unchanged when Coma (A1656) was removed (see Table 3). As expected from that test, there is essentially no change in these results on the ellipticity trends whether Coma is included or removed from the $z < 0.05$ sample.

5. DISCUSSION

We find that neither the median ellipticity nor the shape of the high redshift ellipticity distribution of early-type cluster galaxies evolves with redshift, implying no change in the overall distribution of the bulge-to-disk ratio of early-type galaxies with redshift. As we show in Figure 3, the S0 population at low redshift ($z < 0.05$) has a different ellipticity distribution than the elliptical population, with S0 galaxies having a higher median ellipticity. If the S0 fraction of the early-type galaxy population decreases, then the median ellipticity of the early-type population should decrease. The lack of evolution we observe in the median ellipticity and in the shape of the ellipticity distribution implies little or no evolution in the S0 fraction. This differs from the expectation from previous work, such as that of Dressler et al. (1997), which finds a decrease in the S0 fraction with redshift.

5.1. Morphological Evolution in the $z > 0.3$ Cluster Sample

One possible reason why we may not find any evolution in the ellipticity distribution of the cluster early-type population could be because of the nature of our sample. The fraction of galaxies morphologically selected as S0 galaxies may not change in our sample as has been found by other authors. However, when we look at the S0 fraction of our sample with redshift, using the visual classifications for our sample from the literature, we find a similar trend to what has been reported in other papers, i.e., a lower fraction of S0 galaxies at redshifts $z > 0.4$. In Figure 7, we plot the fraction of morphologically identified S0 galaxies with redshift (from the studies discussed in Section 2.2). Our sample has properties consistent with previous work (Dressler et al. 1997; Fasano et al. 2000; Postman et al. 2005; Desai et al. 2007) as would be expected since our sample largely overlaps with previous studies and uses visual classifications

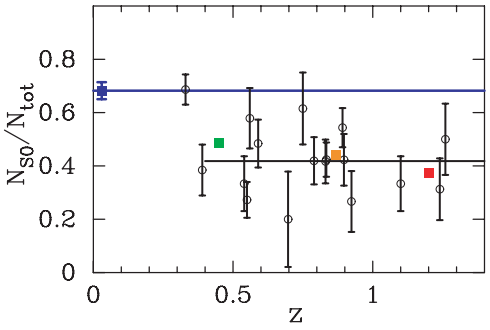

Figure 7. Ratio of morphologically identified S0 galaxies from the studies discussed in Section 2.2 to the total number of elliptical and S0 galaxies. The fraction of S0 cluster galaxies at $z > 0.4$ is lower than that seen at $z < 0.05$, as seen in previous work. We compute the average fraction of S0 galaxies in the early-type population for all of the $z > 0.3$ clusters and plot that value, $42 \pm 2\%$ as a solid black line. For contrast, we show the $z < 0.05$ value, $68 \pm 3\%$, as a solid blue line. We plot, as squares, the average values of the S0 fraction of early-type galaxies in three redshift bins, $0.3 < z < 0.6$ (green), $0.6 < z < 1.0$ (orange) and $z > 1$ (red). Our sample shows the same trend in S0 fraction found by other work. However, the very different fraction of galaxies classified as S0's at $z > 0.4$ is in seeming contradiction with the lack of evolution in the ellipticity distribution.

(A color version of this figure is available in the online journal.)

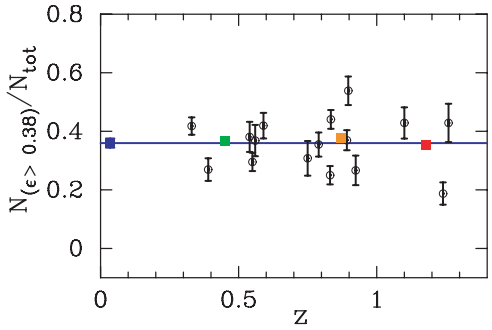

Figure 8. Fraction of cluster early-type galaxies with ellipticities greater than the median ellipticity of the $z < 0.05$ S0 galaxies. The open circles are the fractions of galaxies with $\epsilon_{med} > 0.38$, in each cluster. The squares are the fractions for the $z < 0.05$ (blue), $0.3 < z < 0.6$ (green), $0.6 < z < 1.0$ (orange), and $z > 1$ (red) samples respectively. At low redshift, this fraction has only a small contamination from elliptical galaxies, such that the fraction of galaxies with $\epsilon_{med} > 0.38$ is the half fraction of S0 galaxies with a 5% contamination from elliptical galaxies. If the observed lack of evolution in the median ellipticity of the $z > 0.3$ population is a result of evolution in the ellipticities of elliptical galaxies masking the decline in the S0 population, we should still see a change in the population of galaxies with $\epsilon_{med} > 0.38$. Galaxies with $\epsilon_{med} > 0.38$ represent the most inclined of the disk-dominated early-type galaxies at low redshift. The lack of evolution in this fraction suggests little evolution in the fraction of disk-dominated early-type galaxies as a whole.

(A color version of this figure is available in the online journal.)

from those studies. We find $42 \pm 2\%$ of the early-type galaxy population are S0 galaxies at $z > 0.4$. For comparison, the fraction of S0 galaxies within $2R_{200}/\pi$ for the Postman et al. (2005) "$z \sim 1$ composite" sample is $35 \pm 3\%$. This shows that our red-sequence selection is consistent, being less than 2σ different (the Postman et al. 2005 value is derived by summing the individual listings in that paper's Table 4 under the item labeled "$z \sim 1$ composite").

Our $z < 0.05$ sample of early-type cluster galaxies, selected in the same manner as our $z > 0.3$ sample, has a S0 fraction of $68 \pm 3\%$. This fraction is consistent with other analyses. Examining the whole sample of early-type galaxies within $2R_{200}/\pi$, we find a S0 fraction of $67 \pm 3\%$ for all of the early-type galaxies within for the 10 clusters we use from Dressler (1980a), in good agreement with that found by Dressler et al. (1997). Therefore, our red-sequence selection produces a comparable sample of early-type cluster galaxies to those from previous efforts.

We find no statistically significant evidence for evolution within the $z > 0.4$ cluster sample, which is also consistent with most of the previous work (e.g., Fasano et al. 2000; Postman et al. 2005; Desai et al. 2007). Using the visual classifications, our sample also shows that evolution in the S0 fraction occurs between $z \sim 0$ and $z \sim 0.4$ as the authors above have noted. Note that the fractions we are discussing here are the fraction of S0 galaxies in the early-type galaxy population (see Postman et al. 2005, for a discussion of the size of the systematic error in separating the elliptical and S0 populations).

The result from our measurements of the ellipticity distributions in our clusters is that there is essentially no evolution in the ellipticity distributions from $z \sim 1$ to $z \sim 0$, and thus that there is no change in the overall distribution of the bulge-to-disk ratio of early-type galaxies. If we assume no evolution in the bulge-to-disk ratio distributions of the elliptical and S0 population separately as others have done, we can conclude that the E/S0 ratio does not evolve over this interval. This contrasts with the clear and significant evolution in the S0 fraction seen from many studies (e.g., Dressler et al. 1997; Fasano et al. 2000; Postman et al. 2005; Desai et al. 2007) based on visual classifications. While one explanation is that there is a problem with the visual classifications, this raises an interesting issue. In Postman et al. (2005) and Desai et al. (2007), what evolves at $z > 0.4$ is the fraction of S0 galaxies and the fraction of spiral and irregular galaxies. In contrast, the fraction of elliptical galaxies does not evolve. If the misclassification of round S0 galaxies as ellipticals alone causes the fraction of S0 galaxies to decrease, it is puzzling that there is no corresponding increase in the fraction of elliptical galaxies in Postman et al. (2005) and Desai et al. (2007). Rather, in previous work, the spiral fraction increases, and there is little expectation that face-on S0 galaxies would be misclassified as spirals. The source of this difference remains to be resolved. Our study does not provide an opportunity for a resolution of this issue, but we wanted to highlight it for further work by others.

5.2. Ellipticity by Galaxy Type

Our simulations show that the estimates we use for ellipticities are robust, and do not show a large systematic change with redshift (see Figure 1). Some of the observed change in the fraction of S0 galaxies in Figure 7 may come about from a misclassification of round galaxies as ellipticals, as others (Jørgensen & Franx 1994) have suggested and as we have discussed earlier. It would be useful to examine a sample of S0s for which the elliptical contamination was, likely, very small. We examined the fraction of galaxies with ellipticities above the median of the $z < 0.05$ S0 population, $\epsilon_{med} = 0.38$. Measuring the fraction of galaxies with $\epsilon_{med} > 0.38$ should give us an estimate of the S0 population that we expect to be modestly contaminated by elliptical galaxies. In our $z < 0.05$ sample, we find that $5 \pm 3\%$ of galaxies with $\epsilon > 0.38$ are ellipticals. We plot the fraction of galaxies with $\epsilon_{med} > 0.38$ in Figure 8 as a function of redshift. This once again, shows no change with redshift, implying a S0 fraction that does not evolve under the assumption that the ellipticity distribution of ellipticals and S0 galaxies do not separately evolve.

Table 4
Catalog for CL J1226+33

Obj	R.A. (J2000)	Decl. (J2000)	I (mag AB)	V–I mag AB	z
GAL 12263974+3329315	12:26:39.74	33:29:31.51	21.82 ± 0.02	1.75 ± 0.03	1.035
GAL 12264240+3330094	12:26:42.40	33:30:09.40	22.11 ± 0.01	1.67 ± 0.01	0.929
GAL 12263338+3330277	12:26:33.38	33:30:27.77	21.68 ± 0.01	1.82 ± 0.02	0.911
GAL 12264935+3330312	12:26:49.35	33:30:31.25	21.61 ± 0.01	1.82 ± 0.01	0.891
GAL 12263934+3330353	12:26:39.34	33:30:35.35	22.40 ± 0.01	1.96 ± 0.03	0.943
GAL 12264600+3330347	12:26:46.00	33:30:34.74	21.43 ± 0.01	1.84 ± 0.01	0.892
GAL 12263157+3330473	12:26:31.57	33:30:47.38	22.99 ± 0.02	0.72 ± 0.02	0.963
GAL 12262950+3330580	12:26:29.50	33:30:58.01	21.59 ± 0.01	1.81 ± 0.02	1.211
GAL 12264172+3331041	12:26:41.72	33:31:04.15	22.26 ± 0.01	0.59 ± 0.01	0.690
GAL 12264671+3331037	12:26:46.71	33:31:03.73	22.07 ± 0.01	1.60 ± 0.01	0.767
GAL 12263998+3331047	12:26:39.98	33:31:04.72	21.70 ± 0.01	1.85 ± 0.02	0.929
GAL 12263648+3331124	12:26:36.48	33:31:12.47	22.47 ± 0.02	0.99 ± 0.02	0.846
GAL 12263107+3331349	12:26:31.07	33:31:34.97	22.73 ± 0.01	0.60 ± 0.01	0.965
GAL 12263402+3331356	12:26:34.02	33:31:35.62	21.84 ± 0.01	1.84 ± 0.02	0.966
GAL 12265120+3331385	12:26:51.20	33:31:38.54	22.68 ± 0.01	1.90 ± 0.02	0.881
GAL 12265293+3331465	12:26:52.93	33:31:46.54	22.78 ± 0.01	1.76 ± 0.02	0.964
GAL 12263832+3331482	12:26:38.32	33:31:48.21	23.27 ± 0.06	0.63 ± 0.09	0.542
GAL 12262701+3331580	12:26:27.01	33:31:58.09	22.27 ± 0.08	1.82 ± 0.08	0.645
GAL 12272134+3332083	12:27:21.34	33:32:08.32	21.86 ± 0.01	1.81 ± 0.01	0.893
GAL 12262817+3332232	12:26:28.17	33:32:23.23	22.93 ± 0.02	1.13 ± 0.03	0.673
GAL 12271941+3332269	12:27:19.41	33:32:26.91	23.08 ± 0.02	0.70 ± 0.02	0.885
GAL 12265525+3332324	12:26:55.25	33:32:32.43	22.28 ± 0.01	1.90 ± 0.01	0.895
GAL 12271460+3332377	12:27:14.60	33:32:37.70	22.10 ± 0.01	1.89 ± 0.01	0.881
GAL 12265629+3332414	12:26:56.29	33:32:41.48	22.53 ± 0.01	1.78 ± 0.01	0.893
GAL 12265995+3332405	12:26:59.95	33:32:40.54	22.48 ± 0.01	1.76 ± 0.02	0.892
GAL 12265923+3332405	12:26:59.23	33:32:40.59	22.21 ± 0.01	1.82 ± 0.01	0.897
GAL 12265689+3332437	12:26:56.89	33:32:43.75	22.86 ± 0.01	1.84 ± 0.02	0.896
GAL 12270510+3332475	12:27:05.10	33:32:47.53	23.01 ± 0.01	0.77 ± 0.01	0.798
GAL 12265060+3332461	12:26:50.60	33:32:46.18	21.50 ± 0.01	1.83 ± 0.01	0.875
GAL 12265825+3332485	12:26:58.25	33:32:48.57	19.13 ± 0.00	1.96 ± 0.00	0.891
GAL 12271547+3332539	12:27:15.47	33:32:53.91	22.87 ± 0.02	0.69 ± 0.02	1.034
GAL 12270083+3333019	12:27:00.83	33:33:01.97	22.50 ± 0.01	1.35 ± 0.02	0.914
GAL 12265214+3333071	12:26:52.14	33:33:07.12	23.02 ± 0.02	1.76 ± 0.02	0.881
GAL 12265714+3333046	12:26:57.14	33:33:04.61	21.65 ± 0.01	1.95 ± 0.02	0.930
GAL 12270134+3333044	12:27:01.34	33:33:04.42	21.27 ± 0.00	1.89 ± 0.01	0.897
GAL 12264489+3333094	12:26:44.89	33:33:09.46	22.95 ± 0.01	1.83 ± 0.02	1.196
GAL 12271887+3333137	12:27:18.87	33:33:13.72	21.73 ± 0.01	1.85 ± 0.01	0.897
GAL 12271572+3333111	12:27:15.72	33:33:11.11	21.60 ± 0.01	1.73 ± 0.01	0.892
GAL 12270766+3333138	12:27:07.66	33:33:13.82	22.61 ± 0.01	1.65 ± 0.02	0.902
GAL 12272080+3333163	12:27:20.80	33:33:16.37	21.60 ± 0.01	1.83 ± 0.01	0.819
GAL 12271607+3333192	12:27:16.07	33:33:19.25	22.47 ± 0.02	1.85 ± 0.02	0.901
GAL 12264296+3333195	12:26:42.96	33:33:19.59	22.77 ± 0.01	1.00 ± 0.02	0.849
GAL 12265244+3333239	12:26:52.44	33:33:23.90	22.22 ± 0.02	1.86 ± 0.02	0.893
GAL 12270671+3333266	12:27:06.71	33:33:26.65	21.87 ± 0.01	1.72 ± 0.01	0.883
GAL 12271695+3333261	12:27:16.95	33:33:26.19	21.45 ± 0.01	1.87 ± 0.02	0.891
GAL 12265312+3333310	12:26:53.12	33:33:31.08	21.90 ± 0.01	1.87 ± 0.02	0.896
GAL 12264799+3333348	12:26:47.99	33:33:34.80	22.29 ± 0.01	0.78 ± 0.01	0.330
GAL 12270750+3333439	12:27:07.50	33:33:43.96	22.62 ± 0.01	0.90 ± 0.01	0.850
GAL 12271102+3333471	12:27:11.02	33:33:47.10	21.71 ± 0.01	1.80 ± 0.01	0.755
GAL 12270440+3334063	12:27:04.40	33:34:06.35	22.74 ± 0.01	1.82 ± 0.02	0.887
GAL 12270214+3334060	12:27:02.14	33:34:06.06	21.48 ± 0.01	1.61 ± 0.02	0.896
GAL 12271313+3334130	12:27:13.13	33:34:13.02	21.63 ± 0.01	1.78 ± 0.01	0.763
GAL 12271082+3334195	12:27:10.82	33:34:19.58	22.40 ± 0.01	1.06 ± 0.02	0.767
GAL 12270730+3334237	12:27:07.30	33:34:23.78	22.07 ± 0.01	1.82 ± 0.02	0.892
GAL 12271975+3334272	12:27:19.75	33:34:27.26	21.30 ± 0.01	0.80 ± 0.01	0.530
GAL 12272074+3334437	12:27:20.74	33:34:43.71	21.30 ± 0.01	1.79 ± 0.01	0.762
GAL 12271545+3334558	12:27:15.45	33:34:55.82	21.68 ± 0.01	1.61 ± 0.01	0.768
GAL 12265239+3335006	12:26:52.39	33:35:00.60	22.75 ± 0.01	1.67 ± 0.02	0.764
GAL 12270219+3335182	12:27:02.19	33:35:18.22	22.64 ± 0.02	1.55 ± 0.02	0.891
GAL 12270676+3335289	12:27:06.76	33:35:28.92	21.58 ± 0.01	1.77 ± 0.01	0.755

If the S0 fraction decreases with redshift while the median ellipticity of the early-type population stays the same, we expect that the ellipticity distribution for the S0 galaxies should increase. In Figure 9, we plot the median ellipticity of galaxies

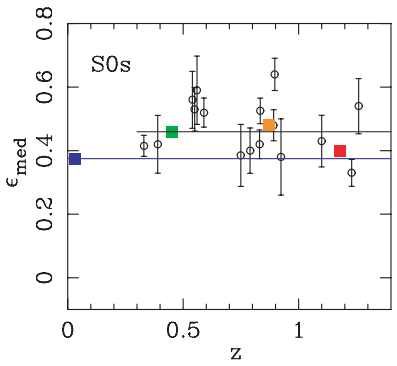

Figure 9. Median ellipticity versus redshift for cluster S0 galaxies. The open circles are the median ellipticities for the galaxies in each cluster. The blue squares are the median for all of the galaxies in the $z < 0.05$ cluster sample. The other squares are the medians for the $0.3 < z < 0.6$ (green), $0.6 < z < 1.0$ (orange), and $z > 1$ (red) samples, respectively. We also show the median value for the $z < 0.05$ S0 sample as a blue line. We show, with a black line, the median ellipticities of all the S0 galaxies in our $z > 0.3$ sample. The median ellipticity of the S0 population increases at $z > 0.3$, with $\epsilon_{med} = 0.47 \pm 0.02$. The median ellipticity of the $z < 0.05$ S0 galaxy is $\epsilon_{med} = 0.38 \pm 0.02$. Such a change in the ellipticity of galaxies classified as S0s can explain how the fraction of galaxies classified as S0's decreases while, at the same time, the median ellipticity of the cluster galaxy population as a whole stays the same.

(A color version of this figure is available in the online journal.)

that are classified visually as S0 galaxies. We show that the median ellipticity of the S0 population is higher in the higher redshift clusters. In the $z > 0.3$ sample, we find that the median ellipticity of the S0 galaxy population is $\epsilon_{med} = 0.47 \pm 0.02$ as compared with $\epsilon_{med} = 0.38 \pm 0.02$ in our $z < 0.05$ low redshift sample[9]. The difference between the $z > 0.3$ and the $z < 0.05$ S0 samples medians is significant at the $> 3\sigma$ when using a Student's *t*-test. Restricting the redshift range to $z > 0.4$, the redshift where other authors have reported that the S0 fraction significant evolves, we find $\epsilon_{med} = 0.48 \pm 0.02$, which is also a $> 3\sigma$ difference. The significance remains $> 3\sigma$ regardless of whether Coma is included in the $z < 0.05$ sample or not.

In Figure 10 (similar to Figure 4, but with just the complete sample with E and S0 identified), we plot the ellipticities as a function of absolute magnitude in four redshift bins. It appears from this figure that there is a deficit of rounder S0 galaxies (blue points) at higher redshifts (excluding the $z > 1$ bin which is less complete and has poor statistics), implying that the S0 galaxies at $z > 0.3$ are drawn from a different distribution than those at $z < 0.05$. The progression of higher ellipticities for the S0 population thus appears to come about from a change in the shape of the ellipticity distribution of S0 galaxies at higher redshift as compared with those at lower redshifts. We discuss this in Section 5.4.

In Figure 11, we quantify what we see in Figure 10. We plot the distributions of the ellipticities for the $z > 0.3$ elliptical and S0 galaxies separately. We find that the shape of the $z > 0.3$ S0 distribution differs from the $z < 0.05$ distribution, in contrast with the elliptical distributions which show little change between the two samples. For example, if we examine the number of S0 galaxies with $\epsilon < 0.3$, we find that there are 56 in the $z > 0.3$ sample, whereas we expect 95 from the scaled low redshift sample of S0 galaxies. We compared the shapes of the two S0 ellipticity distributions using a number of statistical tests. The probability of such a change in the ellipticity distribution of S0 galaxies is $> 3\sigma$ when using a Kolmogorov–Smirnov, Wilcoxon–Mann–Whitney rank sum test and a Kuiper test. These are the same tests that showed no evolution in the ellipticity distribution in Sectiono 4.2. These tests reinforce the result, from the analysis of the trends in Figure 9, that the cluster S0 galaxies have a different ellipticity distribution at $z > 0.3$ than at $z < 0.05$. These trends, both in the median and in the shape of the distribution, are present regardless of how we select the higher redshift sample, whether $z > 0.3$, $z > 0.4$ or $0.4 < z < 1$. In all cases, the distributions differ from the $z < 0.05$ sample at $> 3\sigma$.

Our work is not the only one that finds a different median ellipticity for S0 galaxies at higher redshift in cluster samples. Moran et al. (2007) give the morphological classifications and ellipticities of a sample of S0 galaxies at $z \sim 0.45$. The authors measured the ellipticities of the cluster galaxies using the same approach and software that we use (and thus their ellipticities are PSF corrected). For their cluster S0 galaxies, Moran et al. (2007) find $\epsilon_{med} = 0.48 \pm 0.04$, in excellent agreement with our value of $\epsilon_{med} = 0.48 \pm 0.02$.

Previous work found little or no evolution in the ellipticities of S0 and elliptical galaxies. However, most of the previous work relied on measuring the ellipticities of galaxies using flux-weighted moments of galaxies, without taking into account the "blurring" effects of the PSF or the lower resolution of observations at higher redshifts. We show, in Appendix A, that the ellipticity measurements of galaxies based on simple flux-weighted moments are biased quite significantly towards rounder values for the ACS and WFPC2 data that has been used without correcting for the effects of smoothing by the PSF.

5.3. Constraints on the Evolution of the Bulge-to-Disk Ratio

The observed lack of any evolution in the ellipticity distribution for early-type galaxies has interesting implications for the distribution of the bulge-to-disk ratios of the early-type population from $z \sim 0$ to $z \sim 1$. The average observed ellipticity is directly related to the average intrinsic ellipticity (Binney & Merrifield 1998). If the average bulge-to-disk of a population of galaxies changes, the average intrinsic ellipticity must change too, and vice versa. Our measurement of the an unchanging ellipticity distribution implies that the average bulge-to-disk remains constant.

We performed simple simulations to derive the average ellipticities using models of galaxies with a variety of bulge-to-disk ratios projected over all possible viewing angles with a fixed scale length for the bulges and disk. We find a roughly linear relation between the average bulge-to-total ratio and the average ellipticity of the population. For example, for these simple models, a change in the average bulge-to-total ratio from 0.1 to 0.3, or from 0.3 to 0.6, would be observed as a shift of $\delta\bar{\epsilon} = 0.08$ in the average ellipticity. Such a shift would be a 4σ change for our samples (see Figure 5). While one could potentially develop a model whereby the underlying scale lengths relatively evolve with redshift, this seems rather contrived. "Occam's Razor" would lead one to prefer a model where a constant ellipticity distribution implies a constant distribution of bulge-to-disk ratios over the redshift range from $z \sim 1$ to $z \sim 0$.

[9] These median values are the medians of the all S0 galaxies that meet our selection criteria. These are not the median of the data points we plot in Figure 9. The error we quote is the error on the median, or $\sqrt{(\pi/2)}$ the error on the mean. We confirm these errors with bootstrapping which yields good agreement.

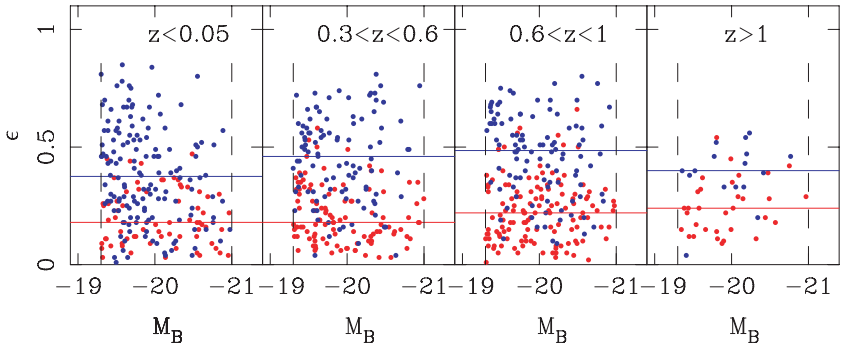

Figure 10. The distribution of ellipticity versus M_B for cluster elliptical (red) and S0 (blue) galaxies in four redshift bins. The solid points are our sample within our magnitude limits of $-19.3 > M_B + 1.208z > -21$. This plot is similar to Figure 4, except that we color code the S0 and elliptical galaxies separately. We show the median values of the populations as lines, red for the ellipticals and blue for the S0 galaxies. We find no statistically significant evolution in the elliptical population. There is a statistically significant ($> 3\sigma$) change in the distribution of ellipticities for S0 galaxies when comparing the $z < 0.05$ S0 population with $\epsilon_{\rm med} = 0.38 \pm 0.02$ and the $0.3 < z < 0.6$ ($\epsilon_{\rm med} = 0.46 \pm 0.02$) or $0.6 < z < 1$ sample ($\epsilon_{\rm med} = 0.49 \pm 0.02$). The uncertainty in the highest redshift sample is too large for any useful comparisons to be made. The change in the ellipticity of the elliptical galaxies with redshift is not statistically significant. From this figure we conclude that the increase in the median ellipticity seen in Figure 9 could arise from a lack of round S0 galaxies at redshifts higher than $z > 0.3$.

(A color version of this figure is available in the online journal.)

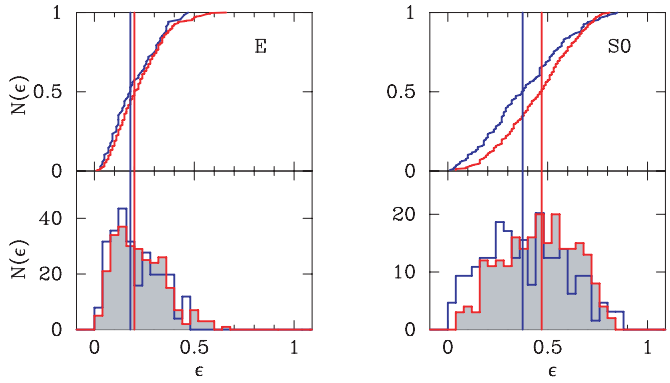

Figure 11. Ellipticity distributions for cluster elliptical (left) and S0 (right) galaxies. The $z < 0.05$ sample is shown in blue, while the $z > 0.3$ sample is shown in red, with the median ellipticity for each shown as a appropriately colored vertical line. We find that the $z > 0.3$ elliptical population is statistically the same as the $z < 0.05$ population. In contrast, there is a statistically significant difference ($> 3\sigma$) in the ellipticities of the S0 population. This appears to be a deficit of round S0 galaxies. We find 56 S0 galaxies with $\epsilon < 0.3$ in our $z > 0.3$ sample, whereas we expect 95 S0 galaxies our $z < 0.05$, after rescaling the $z < 0.05$ to match the total number of S0 expected galaxies. This reinforces Figure 9, showing that the typical ellipticity for S0 galaxies at $z > 0.3$ is higher than at $z < 0.05$ and it appears that there is deficit of round S0 galaxies which is causing this difference in the ellipticity distributions.

(A color version of this figure is available in the online journal.)

5.4. Implications for Evolution in the Fraction of Disk-Dominated Early-type Galaxies

We performed simulations to see if the observed S0 fraction of 42%, for the sample of clusters with $z > 0.4$, is consistent with the lack of evolution we see in the ellipticity distribution. We constructed 10,000 mock catalogs for the clusters in the $z > 0.4$ sample. For each cluster, we assumed that the fraction of S0 galaxies was 42%. We randomly drew the ellipticities for the S0s from the observed distribution of S0s at $z < 0.05$, and drew the ellipticities for the Es from the observed low redshift distribution for Es (see Figure 3). We added the uncertainties and systematics applicable at high redshift as detailed in Section 3.1 and Appendix A.2 The resulting ellipticity distributions had median ellipticities lower than the observed value (0.29) for all 10,000 of the mock catalogs, with a typical value of $\epsilon_{\rm med} = 0.25$. This rules out at $> 4\sigma$ the assumption that the underlying ellipticities and S0 fraction is constant with redshift.

Our others tests which we use to compare the $z < 0.05$ sample and the $z > 0.3$ sample give similar results (the Kolmogorov–Smirnov statistic, a Wilcoxon–Mann–Whitney rank sum statistic and a Kuiper statistic). None of the mock catalogs show the same good agreement between the $z > 0.3$ sample and $z < 0.05$ sample in the ellipticity distribution as we observe.

We repeated these simulations for a variety of S0 fractions. We find that the S0 fraction value that best matches the $z > 0.4$ ellipticity distribution is 66% with a 1σ, or 68% confidence limits, of $\pm 6.5\%$. Another way to consider this is a 1σ change in the median ellipticity at $z > 0.3$, a change of $\delta\epsilon = 0.02$, would imply a change in the S0 fraction of 6.5%. We can rule out, at the 95% confidence limit, S0 fractions below 53%, and we can rule out the observed fraction of visually classified S0 galaxies of $42 \pm 2\%$ at the $> 99.9\%$ confidence limit or at the 4σ level.

To reconcile the evolution seen in the S0 fraction in the visually-classified samples with the lack of evolution in the ellipticity distribution requires that either the S0 and elliptical populations evolve in ellipticity in such a way that the combined samples shows no evolution, or that some fraction of the S0 population has been misclassified as other morphological types (cf. Jørgensen & Franx 1994; Blakeslee et al. 2006).

5.4.1. Possible Spiral Contamination?

One possibility is that the higher ellipticity, or more edge-on, S0 population is contaminated with misclassified red spirals. This would cause the S0 fraction to be overestimated, while, at the same time change the shape of the ellipticity distribution. The spiral fraction among galaxies in the mass range of the cluster sample in our work is $\sim$ 10%–15% (Holden et al. 2007) while the fraction of dusty, red objects is $\sim$ 10% (Saintonge et al. 2008). Since the misclassification would be predominately for edge-on systems, these fractions are likely upper limits for the fraction of spirals misclassified as S0 galaxies. Is it possible that such a small fraction of "spiral" galaxies could contaminate the population visually classified as S0 galaxies and change the ellipticity distribution at higher redshift?We examined the ellipticities of the galaxies classified as spirals in both the $z < 0.05$ and $z > 0.3$ sample to see if there is a deficit of edge-on spirals. We found the opposite, that there is a shift in the high redshift spiral population to larger

ellipticities, $\epsilon_{\rm med} = 0.38 \pm 0.04$ at $z < 0.05$ (as expected, see Ryden 2006) to $\epsilon_{\rm med} = 0.45 \pm 0.03$ at $z > 0.3$, but it is not statistically significant. From this we conclude that a red spiral population is not a major source of contamination, especially at large ellipticities.

Given the quantitative nature of the current study we feel that it provides a key datum for consideration of the evolutionary history of early-type galaxies over the last 8 Gyr. The result that the ellipticity distribution is essentially unchanged from $z \sim 0$ to $z \sim 1$, combined with the result that the fraction of highly elongated disk-dominated systems does not evolve (see Figure 8), provides strong evidence that the overall bulge-to-disk ratio distribution of the population does not evolve.

6. SUMMARY AND IMPLICATIONS

We have compiled a sample of 10 $z > 0.05$ clusters of galaxies and a comparable sample of 17 $z > 0.3$ clusters of galaxies with *HST* imaging. For each cluster, we selected a subsample of galaxies that lie on the red sequence and have been classified as an early-type galaxy (elliptical or S0 galaxy). To derive a robust sample at all redshifts, we selected galaxies to fall within a magnitude range of $-19.3 > M_B + 1.208z > -21$ and required the galaxies to lie within $2R_{200}/\pi$ (to ensure that the de-projected sample lies within R_{200}) of the cluster center. We change the rest-frame B magnitudes by $1.208z$ to match the mass-to-light evolution of cluster early-type galaxies as measured by the fundamental plane (van Dokkum & van der Marel 2007). The magnitude limits correspond to $M_B^* + 1 > M_B > M_B^* - 0.75$ or galaxies with stellar masses roughly between $10^{10.6}\ M_\odot < M < 10^{11.2}\ M_\odot$, assuming a "diet" Salpeter IMF.

We performed extensive simulations of the ellipticity measurements to test their robustness and to minimize systematics with redshift. We found that it is crucial to use model fits (e.g., GALFIT) where the effect of the PSF can be modeled and removed. From our extensive simulations we find that we can robustly measure the ellipticity of cluster early-type galaxies (by using PSF-corrected model fits) out to $z \sim 1.3$ at magnitudes that allow the galaxies to also be morphologically classified. The systematic error we find in our simulations is only $\delta_\epsilon = -0.01$, or a 3% change for the median galaxy. We do not apply this small correction to our data. We find that not including the effect of the PSF can cause systematic shifts of $\delta_\epsilon = -0.10$, or a 30% change for the median galaxy.

Using our two samples of cluster early-type galaxies, we measure the evolution in the ellipticity of $z > 0.3$ cluster early-type galaxies compared with a substantial sample at $z < 0.05$.

1. We find no evolution in the median ellipticity of $z > 0.3$ cluster early-type (elliptical and S0) galaxies relative to the low redshift sample. The median ellipticity at $z < 0.05$ is $\epsilon_{\rm med} = 0.29 \pm 0.02$, and is $\epsilon_{\rm med} = 0.30 \pm 0.01$ at $z > 0.3$. *The median ellipticity of our sample of 487 early-type galaxies at* $z > 0.3$ *is statistically the same as that of the 210 early-type galaxies at* $z < 0.05$*, being higher by only* 0.01 ± 0.02 *or* $3 \pm 6\%$.
2. The shape of the ellipticity distribution of $z > 0.3$ galaxies also does not evolve. *The distribution of ellipticities at* $z > 0.3$ *agrees with the shape of the* $z < 0.05$ *distribution at the 1%–2% level (i.e., the probability that they are drawn from the same distribution is 98%–99%).*
3. Using visual classifications from previous reference studies, we find that our sample shows a similar decrease in the fraction of early-type galaxies classified as disk-dominated systems (S0s) at $z > 0.4$. As other studies have found, t he S0 fraction is $68 \pm 3\%$ at $z < 0.05$ and decreases to $42 \pm 2\%$ at $z > 0.4$.
4. For the S0 fraction to decrease with increasing redshift, while the median ellipticity of the overall cluster early-type population stays the same, the median S0 ellipticity needs to be larger at higher redshift. There is a trend in our data for $z > 0.3$ in this sense. The median S0 galaxy at $z < 0.05$ is $\epsilon_{\rm med} = 0.38 \pm 0.02$ while at $z > 0.3$, we find a $\sim 3\sigma$ different $\epsilon_{\rm med} = 0.47 \pm 0.02$ for galaxies classified as S0s. Whether this change is large enough to account for the change seen in the morphological sample remains to be determined. We explored if the change in the ellipticity distribution of S0 galaxies could come from a deficit of round S0 galaxies or from the addition of misclassified spiral galaxies. However, we found that neither of these simple scenarios can explain our results.

Our results on the unchanging ellipticity distributions lead us to conclude that there has been little or no evolution in the overall distribution of bulge-to-disk ratio of early-type galaxies over the redshift range $0 < z < 1$ for morphologically-selected samples of early-type red-sequence galaxies with $M_B^* + 1 > M_B > M_B^* - 0.75$ in the dense cores of clusters inside R_{200}. In particular, our results allow us to rule out a S0 fraction of <47%–51% at $z > 0.3$ at the 3σ level assuming no evolution in the ellipticity distributions of elliptical and S0 galaxies. *If we assume, as in all previous studies, that the intrinsic ellipticity distribution of both elliptical and S0 galaxies remains constant, then we conclude from the lack of evolution in the observed early-type ellipticity distribution that the relative fractions of ellipticals and S0s do not evolve over the last* ~ 8 *Gyr, or from* $z \sim 1$ *to* $z = 0$*, for a red-sequence selected samples of early-type galaxies in the cores of clusters of galaxies.*

These results do highlight an inconsistency within the wide range of studies that have occurred on the evolution of early-type galaxies over the last decade. Over this redshift range, and particularly since $z \sim 0.4$, the fraction of morphologically-identified S0 galaxies from visual classifications has been found to be significantly lower than the $z \sim 0$ value (see, e.g., Dressler et al. 1997; Fasano et al. 2000; Postman et al. 2005; Desai et al. 2007). Reconciling the trends seen in the elliptical, S0 and spiral fractions, as discussed in Section 5.1 remains to be understood.

The early-type galaxy population, both in the field and in clusters, does not evolve purely passively. The volume-averaged number density of red galaxies, which are mostly early-type galaxies (Bell et al. 2004a), grows by a factor ~ 2 between $z \sim 1$ and the present (Bell et al. 2004b; Brown et al. 2007; Faber et al. 2007). For the cluster population such evolution is harder to quantify, but mergers (van Dokkum et al. 1999; Tran et al. 2005) and filaments around massive clusters at $z \sim 0.8$ (e.g., Kodama et al. 2005; Patel et al. 2009) suggest that interactions and infalling galaxies enhance and modify over time the galaxy population in the cluster core. Besides evolution in the population of early-type galaxies, individual early-type galaxies also change over time. As pointed out by, e.g., Jørgensen et al. (2005), the evolution of the line strengths is not compatible with purely passive evolution. Moreover, recently, early-type galaxies at $z \sim 1$ were recently demonstrated to be significantly smaller than today by a factor of two van der Wel et al. (2008). Hence, the arising picture is complicated: early-type galaxies, both as individual objects and as a population, undergo substantial changes between $z \sim 1$ and the present.

On the other hand, many basic properties of the early-type population have remained unchanged over the past ~ 8 Gyrs, providing useful means for characterizing and quantifying the observed evolution. At any redshift $z \sim 1$ early-type galaxies occupy a tight color-magnitude relation (e.g., Blakeslee et al. 2006) and fundamental plane (e.g., Wuyts et al. 2004), which suggests smooth and regular evolution. Moreover, neither in the field nor in clusters has the early-type *fraction* changed significantly in mass-selected samples (Holden et al. 2007; van der Wel et al. 2007). Together with these characteristics, the results presented in this paper fit into a picture in which the field and cluster early-type galaxy populations grow and change, but only while leaving many basic characteristics the same. In particular, we have demonstrated from the constancy of the ellipticities of early-type galaxies over the last ~ 8 Gyr that the bulge-to-disk ratio distribution of the cluster population remains constant. This suggests that processes that change the bulge-to-disk ratio of individual early-type galaxies and the bulge-to-disk ratios of newly formed or accreted early-type galaxies are balanced such that the overall bulge-to-disk ratio distribution remains the same. It remains an open question why this is the case, but it is clear that much can be learned about the formation process of early-type galaxies by studying their properties in even more detail and extending their observation to higher redshifts.

The authors would like to thank S. Adam Stanford for useful comments. We would also like to thank the anonymous referee for uesful suggestions that improved this paper. Finally, we would like to thank Stefano Andreon for pointing out previously published related papers, and Dave Wilman for showing us his work ahead of publication. ACS was developed under NASA contract NAS5-32865, this research was supported by NASA grant NAG5-7697. We are grateful to K. Anderson, J. McCann, S. Busching, A. Framarini, S. Barkhouser, and T. Allen for their invaluable contributions to the ACS project at JHU. This research has made use of the NASA/IPAC Extragalactic Database (NED) which is operated by the Jet Propulsion Laboratory, California Institute of Technology, under contract with the National Aeronautics and Space Administration. The analysis pipeline used to reduce the DEIMOS data was developed at UC Berkeley with support from NSF grant AST-0071048.

Facilities: HST (ACS, WFPC2) Magellan:Baade (LDSS2, IMACS), Keck:I (LRIS) Keck:II (DEIMOS)

APPENDIX A

ROBUSTNESS OF ELLIPTICITY MEASUREMENTS

We made a number of additional tests of the robustness of the ellipticity measurements with the goal of estimating the magnitude of any systematic errors. These include adding fake galaxies into our imaging data, comparing the ellipticity measurements made using SExtractor to those using GALFIT, and using the a range of (incorrect) PSFs to estimate the possible sensitivity to systematic errors.

A.1. Simulations with Fake Galaxies

We performed a number of simulations using fake galaxies to test the reliability of the ellipticity measurements. These simulations were done in order to establish the best approach to use and to assess how well we can measure the ellipticity, given our data.

The artificial galaxies were made by simulating two Sérsic models with the same centroid, one with $n = 4$ and one with $n = 1$. The two components had the same luminosity, but different effective radii. The first effective radius was chosen to be three times the resolution of the ACS camera, while the second was nine times the ACS resolution. Each component was given the same ellipticity. These represent well-resolved lenticular galaxies. These fake images were then simulated at magnitudes typical of the early-type galaxies in the $z \sim 0.8$–0.9 clusters in our ACS imaging, and then added to a real ACS image. Reassuringly, the simulations recovered the input ellipticities to a high accuracy, with a scatter of just $\sigma_e/e = 0.027$ and an offset of $\delta_e/e = -0.0007$. The scatter and the offset was highest for the most round objects. For objects with an input ellipticity of 0, the average recovered ellipticity was 0.03 with a scatter of $\sigma_e = 0.014$. As expected, objects that would be seen as perfectly round given an arbitrarily high signal-to-noise, are not measured to be round at typical signal-to-noise levels, but the offset, as noted above, was quite small.

These simulations were made for a variety of bulge-to-disk ratios, by varying the relative luminosities of the two components. In addition, we assumed that the intrinsic ellipticity of the $n = 4$ bulge was $\epsilon = 0.3$, or $\bar{\epsilon} = 0.2$ when averaged over all projections or over all $\cos(i)$.

A.2. Simulations with Real Galaxies

We compiled a number of images of low redshift elliptical and S0 galaxies. We began with the catalog of Frei et al. (1996). That catalog contains 24 elliptical and S0 galaxies, including two classified as S0/a. We expanded upon this by including 49 additional early-type galaxies in the Virgo cluster. Each was selected to be in the Virgo cluster sample discussed in Mei et al. (2007). Most of the galaxies in that sample have accurate distances from surface brightness fluctuations. Those that do not have distances were assumed to be at the center of the main Virgo concentration.

Once we selected the list of early-type galaxies, we extracted images of those not in Frei et al. (1996) from the SDSS DR5 in the g filter. For those images from the SDSS, we removed nearby bright stars and other galaxies, replacing the pixels with those randomly selected from nearby blank regions. This produced a final collection of 73 images of nearby galaxies imaged in either g or B.

We added these galaxies, appropriately scaled in size and magnitude, to the imaging data used for each of the clusters, and replicated the detection and measuring process. The galaxies were resized as appropriate for the redshift of the cluster, convolved with a representative PSF, and then noise was added to each. Each galaxy was simulated at a variety of input magnitudes, and multiple realizations were done at each magnitude to evaluate the effect of noise and binning. This is the same process used in Holden et al. (2004). The magnitudes were selected to span the range of observed galaxy magnitudes, to 0.4 mag below the limit used for classifying galaxies in each sample. This is important to ensure that the selection at the limit is not influenced by the magnitude cutoff.

A.2.1. Recovery of the Input Galaxy's Ellipticity

We compared the offset between the ellipticity measurement from the original image and that of the simulated high redshift image. In general, the offset between the low redshift original image and high redshift scaled image ellipticities are consistent. For galaxies within our magnitude limits, we found that the

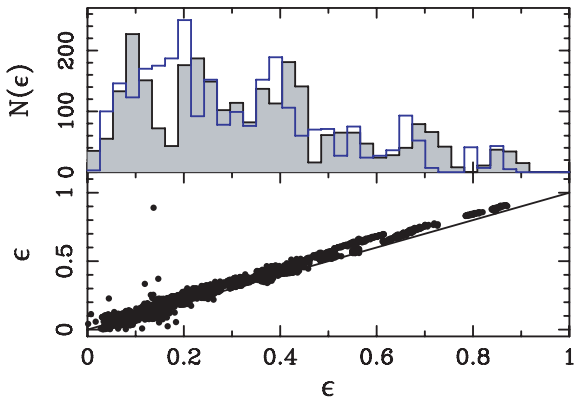

Figure 12. Ellipticity determined with wrong PSF versus ellipticity with the correct PSF. The bottom panel shows the output ellipticity as a function of the input ellipticity, with a line with a slope of one to guide the eye. The top panel shows the input ellipticity distribution in blue and the output as the gray-shaded histogram. The simulations were done for cluster galaxies at $z = 0.83$ which were convolved with the i_{775} PSF, but the modeling of the galaxy luminosity profiles was done using the I_{814} PSF has some asymmetry. The use of the incorrect PSF in this case has only a modest impact, biasing the ellipticities towards higher values by $\delta_\epsilon \sim 0.03$ at the highest ellipticities and becomes smaller, $\delta_\epsilon = 0.018$ or a ∼6% change, at the median input ellipticity.

(A color version of this figure is available in the online journal.)

typical systematic offset is from $\delta_\epsilon \sim -0.03$ to $\delta_\epsilon \sim 0.01$, where the simulated galaxies are measured to be less elliptical at high redshift than in their original, low redshift images. For galaxies at or below our selection limits $\delta_\epsilon \sim -0.06$ to $\delta_\epsilon \sim 0.05$. The median systematic offset was $\delta_\epsilon \sim 0.01$ for our whole sample of simulated galaxy images. We show the ellipticities measured in the output of the simulations as a function of the input ellipticities in Figure 1. The scatter scales with the input signal-to-noise as expected. One exception is that, in general, the measurements made with WFPC2 are worse than those made with ACS at the same redshift. This is expected, because WFPC2 is under-sampled and the images are typically at a lower S/N.

A.2.2. Random Errors

We used the multiple realizations of the galaxy simulations to examine the random errors. The scatter in the measurements for a given input galaxy in a given cluster observation is, on the whole, small. The ACS imaging has measurements with a median scatter of $\sigma_\epsilon \sim 0.01$ in ellipticity, while the WFPC2 imaging shows larger median scatter of $\sigma_\epsilon \sim 0.02$–$0.03$ in ellipticity. These numbers are close to the typical errors reported by GALFIT. GALFIT's reported errors scale with the magnitude of the galaxy, which we also find in our simulations. At the faintest magnitudes, at or below the magnitude limits for classification, we find a scatter on the ellipticities as high as $\sigma_\epsilon \sim 0.05$, once again matching the scatter in the ellipticity as estimated by GALFIT.

A.2.3. Systematic Errors from PSF Mismatches

Because the PSF is so important, we performed simulations where GALFIT was run using a different PSF than the PSF that was used to convolve with the data. We reran the simulations for MS 1054−03 using the correct i_{775} PSF when simulating the $z = 0.83$ galaxy, but we ran GALFIT using the I_{814} PSF. The differences between all three PSFs in terms of encircled energy are small (Sirianni et al. 2005). However, there is an asymmetry in the PSF of the I_{814} filter (Sirianni et al. 2005; Jee et al. 2007) that causes a noticeable difference in the resulting PSFs.

We show the results of using the I_{814} PSF to fit in Figure 12. We find an overall offset of $\delta_\epsilon \sim 0.027$ between the average ellipticities, which is of order the same size as the bins we use in the top panel. Examining the lower panel, we can see that the offset is not constant with ellipticity, but also depends on the input galaxy used for the simulation. For example, along the x-axis at $\epsilon \sim 0.3$, there are a number of points where the incorrect PSF yields $\epsilon \sim 0.4$ while other galaxies have similar ellipticities when using the correct or incorrect PSF. From this we can conclude that typical systematic errors on the ellipticity measurements are on the order of $\delta_\epsilon \sim 0.01$–$0.03$, but this depends on the shape of the galaxy. The PSF is more asymmetric in the redder passbands, so the systematic error is likely to be largest for the highest redshift clusters. The statistic we use the most is the median ellipticity. Using these simulations, we find that the offset in the median ellipticity is $\delta_\epsilon = 0.018$ for the I_{814} data. This is a quite a small effect, given the noticeable changes that we have made to the PSF.

A.3. Comparison of Ellipticity Measures

Previous work, such as Dressler et al. (1997) and Postman et al. (2005), use SExtractor's flux-weighted moments to estimate the ellipticities of galaxies. This approach, however, does not remove the effect of the PSF. Below we will compare the ellipticity measurements we use with those used by previous work in the literature. We will also use our simulations to evaluate how well these techniques reproduce the underlying ellipticity distribution.

In Figure 13, we compare our ellipticity measurements for CL 0016+16 CL 0024+16 and CL 0054−27 with those from Smail et al. (1997). Our measurements, as we stated above, are based on fitting elliptical models of Sérsic profiles to the data, including the effects of the PSF. The results from Smail et al. (1997) are based on using SExtractor (Bertin & Arnouts 1996). SExtractor estimates the ellipse by computing the flux-weighted second-order moments of the galaxy. SExtractor includes those pixels above the threshold defined by an isophote as measured in a smoothed image. Smail et al. (1997) used a detection isophote of $\sim 1.3\sigma$ and a 0.″3 diameter, or 3 pixels with WFPC2, top-hat filter for the smoothing.

We find that our ellipticities are less round than those from Smail et al. (1997). We hypothesize that this comes about for two reasons. First, our approach removes the smoothing from the PSF which tends to circularize the ellipticity measurements. Second, much of our data was observed with ACS, which has a more compact PSF than WFPC2. The median offset in the ellipticities for S0 galaxies is $\delta\epsilon_{\rm med} = -0.13$. This is a very large change, much larger than any of the systematic error we found in our simulations of our ellipticity measurements. This highlights the importance of including the PSF in the measuring process, and does indicate the challenge of using WFPC2 data for measurements at higher redshift.

In Figure 14, we plot the ellipticities we measure using SExtractor on the ACS images of MS 1054−03 and CL 0024+16 in comparison to the ellipticities we find by fitting models using GALFIT. From these plots, we conclude that the more compact PSF for ACS is not the dominate reason for the different ellipticities between our work and the work of previous authors. Removing the effect of the PSF is the most important component.

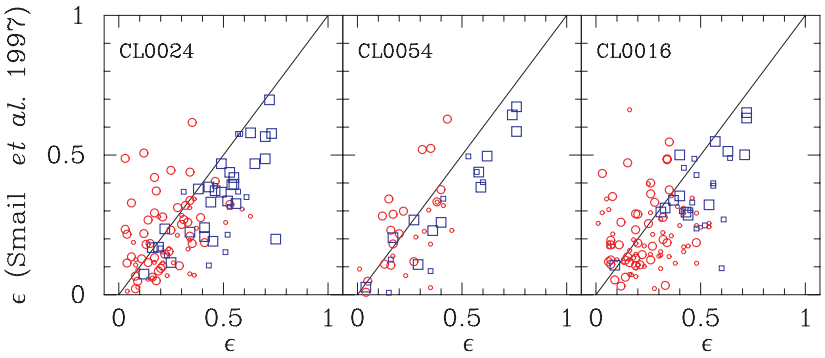

Figure 13. Ellipticity measurement comparison with Smail et al. (1997). Our ellipticities measured by fitting PSF convolved models to the images with GALFIT are on the *x*-axis. The *y*-axis values are ellipticities from Smail et al. (1997) measured from the second-order flux-weighted moments of galaxies using SExtractor. Galaxies classified by eye as S0s are open blue squares while ellipticals are red circles. The smaller symbols are galaxies with radii less than 0.″3, or ∼ 2 WFPC2 resolution elements. The black line is a line of slope one with an intercept of zero. Our ellipticities are generally less round than those of Smail et al. (1997), and this is discrepancy is larger for the smaller galaxies. The median offset in the ellipticities for S0 galaxies is $\delta\epsilon_{\rm med} = -0.13$, much larger than the worst systematic error we found in our simulations of our ellipticity measurements. This highlights the importance of including the PSF in the measuring process.

(A color version of this figure is available in the online journal.)

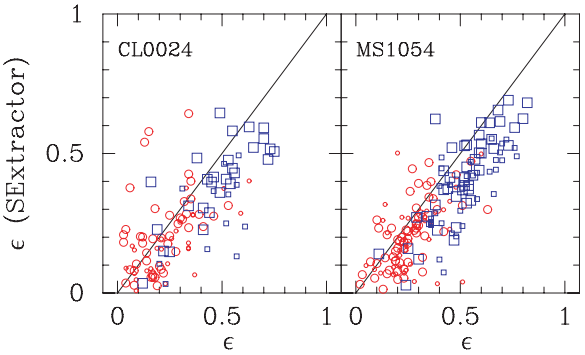

Figure 14. SExtractor measures of the ellipticity versus those from GALFIT for ACS imaging data. This plot is similar to Figure 13, and uses the same symbols, but compares ellipticities from measurements of the second-order flux-weighted moments made with ACS imaging, as opposed to WFPC2 as in Figure 13, to those from fitting models to the galaxies. As we see in Figure 13, the luminosity-weighted moment estimates are generally rounder than the ones measured by GALFIT model fitting, despite the higher resolution and better sampling of ACS as compared with WFPC2. This figure shows that modeling the PSF when measuring the ellipticity is particularly important for deriving a robust estimate of the underlying value, and that the resolution of the instrument is a lesser factor (at least in this case between WFPC2 and ACS). As in Figure 13, the galaxies classified as S0s are more likely to have small ellipticities when they are larger in size. The median offset for S0 galaxies is $\delta\epsilon_{\rm med} = -0.10$, smaller than we found in Figure 13, but still much larger than the statistical and systematic errors we find for our PSF-corrected GALFIT model approach.

(A color version of this figure is available in the online journal.)

Finally, we plot the comparison between the ellipticities as derived by GALFIT and those from SExtractor in Figure 15 for our simulations of high-redshift galaxies. These are images of real galaxies that have been redshifted and to which we have added noise. As with the previous plots showing trends in the data, the simulated galaxies are measured to be rounder with SExtractor than by fitting models using GALFIT. The average offset is $\delta\epsilon_{\rm med} \sim -0.09$ between the SExtractor ellipticity and the GALFIT ellipticity, in good agreement with the $\delta\epsilon_{\rm med} = -0.10$ we measure in Figure 14. As we show in Figure 1, our GALFIT ellipticities reproduces the underlying ellipticity distribution. Because our GALFIT method reproduces the input ellipticities so well, we conclude that the SExtractor method of measuring ellipticities underestimates the ellipticities of galaxies at higher redshifts. We would advise against the use of SExtractor ellipticities for quantitative studies of high redshift galaxies using ACS and WFPC2 where the PSF is a modest, but significant fraction of the size of the object.

APPENDIX B

THE REDSHIFT CATALOG FOR CL J1226+33

Of the clusters discussed here, only CL J1226+33 has no previously published redshift catalog beyond the six galaxies listed in the discovery paper (Ebeling et al. 2001). We have

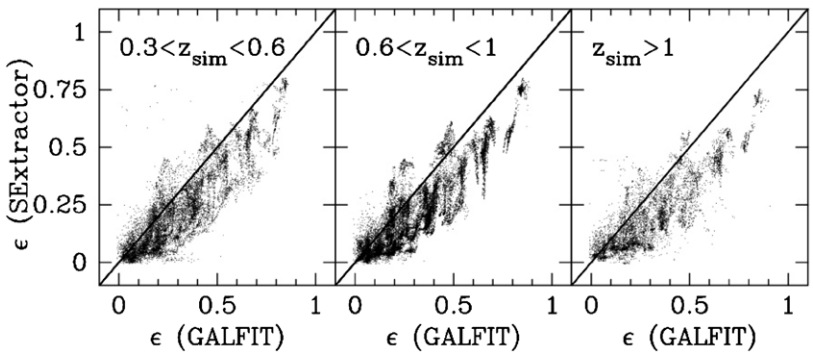

Figure 15. SExtractor ellipticities as a function of the GALFIT ellipticities for galaxies from our simulations. We plot the SExtractor ellipticities on the *y*-axis as a function of the GALFIT ellipticities for the same simulated galaxies. For comparison, we plot a line with a slope of one. Note that this plot shows a similar behavior as Figures 13 and 14, namely that the ellipticities as estimated by SExtractor are rounder than those from GALFIT. The GALFIT measurements of the simulated $z > 0.3$ galaxies recover the actual ellipticities with an average offset of $\delta_\epsilon \sim -0.01$ (see Figure 1), much smaller than the offset of $\delta_\epsilon \sim -0.09$ we find between the GALFIT and SExtractor ellipticities. The higher density of points in the $z = 0.85$ redshift bin simply reflects the larger number of clusters included in that bin.

collected redshifts for 21 new members in the central region of the cluster, along with 10 more galaxies outside of the region covered by the ACS imaging. 30 of these 31 galaxies were selected to have ACS I_{814} magnitudes < 24 mag AB and colors in the range $1.5 < V_{606} - I_{814} < 2$, the remaining one was a "filler" object with a bluer color. The data were taken using the DEIMOS spectrograph on Keck II, in a 1 hr exposure with the 600 line mm^{-1} grating in variable conditions. We list the catalog of redshifts in Table 4.

We measured redshifts by centroiding emission features and cross-correlating with a variety of templates. We computed the biweight center and scale of all galaxies with redshifts within $0.87 < z < 0.91$. We found $\bar{z} = 0.890 \pm 0.001$ with a dispersion of 1143 ± 162 km s^{-1}, in good agreement with the 1270 km s^{-1} quoted in Jørgensen et al. (2006). We used a biweight to estimate both the redshift and the velocity dispersion of the cluster with errors from the jackknife of the galaxy redshifts. The redshift range we used for membership excludes two galaxies at $z \sim 0.91$. Including those two objects raises the dispersion to 1322 ± 221 km s^{-1}. It is often the case that, with small numbers of galaxies that the dispersion is overestimated–see, for example, the dispersions quoted for CL 1604+4304 and CL 1604+4321 in Lubin et al. (2000) versus those from the much larger sample in Gal et al. (2005). This arises because nearby large scale structure or groups of galaxies can project into line of sight of the cluster. We opted to remove the two galaxies at $z \sim 0.91$ to provide conservative estimate of the dispersion, which we also list in Table 2.

REFERENCES

Abell, G. O., Corwin, H. G. J., & Olowin, R. P. 1989, ApJS, 70, 1
Adelman-McCarthy, J. K., et al. 2007, ApJS, 172, 634
Andreon, S. 1998, ApJ, 501, 533
Andreon, S., Davoust, E., Michard, R., Nieto, J.-L., & Poulain, P. 1996, A&AS, 116, 429
Bell, E. F., McIntosh, D. H., Katz, N., & Weinberg, M. D. 2003, ApJS, 149, 289
Bell, E. F., et al. 2004a, ApJ, 600, L11
Bell, E. F., et al. 2004b, ApJ, 608, 752
Bertin, E., & Arnouts, S. 1996, A&AS, 117, 393
Binney, J., & Merrifield, M. 1998, in Princeton Series in Astrophysics Galactic Astronomy, ed J. Binney & M. Merrifield (Princeton, NJ: Princeton Univ. Press)
Blakeslee, J. P., Anderson, K. R., Meurer, G. R., Benítez, N., & Magee, D. 2003, in ASP Conf. Ser. 295, Astronomical Data Analysis Software and Systems XII (San Francisco, CA: ASP), 257
Blakeslee, J. P., et al. 2006, ApJ, 644, 30
Brown, M. J. I., Dey, A., Jannuzi, B. T., Brand, K., Benson, A. J., Brodwin, M., Croton, D. J., & Eisenhardt, P. R. 2007, ApJ, 654, 858
Bruzual, G., & Charlot, S. 2003, MNRAS, 344, 1000
Buser, R. 1978, A&A, 62, 411
Butcher, H., & Oemler, A. 1984, ApJ, 285, 426
Carlberg, R. G., Yee, H. K. C., & Ellingson, E. 1997, ApJ, 478, 462
Carlberg, R. G., Yee, H. K. C., Ellingson, E., Abraham, R., Gravel, P., Morris, S., & Pritchet, C. J. 1996, ApJ, 462, 32
Demarco, R., et al. 2005, A&A, 432, 381
Demarco, R., et al. 2007, ApJ, 663, 164
Desai, V., et al. 2007, ApJ, 660, 1151
Dressler, A. 1980a, ApJS, 42, 565
Dressler, A. 1980b, ApJ, 236, 351
Dressler, A., & Gunn, J. E. 1992, ApJS, 78, 1
Dressler, A., Smail, I., Poggianti, B. M., Butcher, H., Couch, W. J., Ellis, R. S., & Oemler, A. J. 1999, ApJS, 122, 51
Dressler, A., et al. 1997, ApJ, 490, 577
Ebeling, H., Jones, L. R., Fairley, B. W., Perlman, E., Scharf, C., & Horner, D. 2001, ApJ, 548, L23
Faber, S. M., et al. 2007, ApJ, 665, 265
Fabricant, D., Franx, M., & van Dokkum, P. 2000, ApJ, 539, 577
Fasano, G., Poggianti, B. M., Couch, W. J., Bettoni, D., Kjærgaard, P., & Moles, M. 2000, ApJ, 542, 673
Finn, R. A., et al. 2005, ApJ, 630, 206
Fisher, D., Fabricant, D., Franx, M., & van Dokkum, P. 1998, ApJ, 498, 195
Franx, M., Illingworth, G., & de Zeeuw, T. 1991, ApJ, 383, 112
Frei, Z., Guhathakurta, P., Gunn, J. E., & Tyson, J. A. 1996, AJ, 111, 174
Gal, R. R., Lubin, L. M., & Squires, G. K. 2005, AJ, 129, 1827
Halliday, C., et al. 2004, A&A, 427, 397
Högbom, J. A. 1974, A&AS, 15, 417
Holden, B. P., Stanford, S. A., Eisenhardt, P. R., & Dickinson, M. 2004, AJ, 127, 2484
Holden, B. P., et al. 2005, ApJ, 626, 809
Holden, B. P., et al. 2006, ApJ, 642, L123
Holden, B. P., et al. 2007, ApJ, 670, 190
Hubble, E. P. 1936, The Realm of the Nebulae (New Haven, CT: Yale Univ. Press)
Jee, M. J., Blakeslee, J. P., Sirianni, M., Martel, A. R., White, R. L., & Ford, H. C. 2007, PASP, 119, 1403
Jørgensen, I., Bergmann, M., Davies, R., Barr, J., Takamiya, M., & Crampton, D. 2005, AJ, 129, 1249
Jørgensen, I., Chiboucas, K., Flint, K., Bergmann, M., Barr, J., & Davies, R. 2006, ApJ, 639, L9
Jørgensen, I., & Franx, M. 1994, ApJ, 433, 553
Kodama, T., et al. 2005, PASJ, 57, 309
Kormendy, J., & Djorgovski, S. 1989, ARA&A, 27, 235
Krajnovic, D., et al. 2008, MNRAS, 390, 93
Krist, J. 1995, in ASP Conf. Ser. 77, Astronomical Data Analysis Software and Systems IV (San Francisco, CA: ASP), 349
Limber, D. N., & Mathews, W. G. 1960, ApJ, 132, 286
Lubin, L. M., Brunner, R., Metzger, M. R., Postman, M., & Oke, J. B. 2000, ApJ, 531, L5
Mei, S., et al. 2006a, ApJ, 639, 81
Mei, S., et al. 2006b, ApJ, 644, 759
Mei, S., et al. 2007, ApJ, 655, 144
Mei, S., et al. 2009, ApJ, 690, 42
Moran, S. M., Loh, B. L., Ellis, R. S., Treu, T., Bundy, K., & MacArthur, L. A. 2007, ApJ, 665, 1067
Norberg, P., et al. 2002, MNRAS, 336, 907
Patel, S. et al. 2009, ApJ, in press
Peng, C. Y., Ho, L. C., Impey, C. D., & Rix, H.-W. 2002, AJ, 124, 266
Poggianti, B. M., et al. 2006, ApJ, 642, 188
Postman, M., et al. 2005, ApJ, 623, 721
Rix, H.-W., & White, S. D. M. 1990, ApJ, 362, 52
Rood, H. J., & Baum, W. A. 1967, AJ, 72, 398
Ryden, B. S. 2006, ApJ, 641, 773
Saintonge, A., Tran, K.-V. H., & Holden, B. P. 2008, ApJ, 685, L113
Sandage, A., Freeman, K. C., & Stokes, N. R. 1970, ApJ, 160, 831
Sirianni, M., et al. 2005, PASP, 117, 1049
Smail, I., Ellis, R. S., Dressler, A., Couch, W. J., Oemler, A. J., Sharples, R. M., & Butcher, H. 1997, ApJ, 479, 70
Smith, G. P., Treu, T., Ellis, R. S., Moran, S. M., & Dressler, A. 2005, ApJ, 620, 78
Stanford, S. A., Holden, B., Rosati, P., Tozzi, P., Borgani, S., Eisenhardt, P. R., & Spinrad, H. 2001, ApJ, 552, 504
Struble, M. F., & Rood, H. J. 1999, ApJS, 125, 35
Tran, K. H., Franx, M., Illingworth, G., Kelson, D. D., & van Dokkum, P. 2003, ApJ, 599, 865
Tran, K. H., van Dokkum, P., Franx, M., Illingworth, G. D., Kelson, D. D., & Schreiber, N. M. F. 2005, ApJ, 627, L25
Tran, K.-V. H., Franx, M., Illingworth, G. D., van Dokkum, P., Kelson, D. D., Blakeslee, J. P., & Postman, M. 2007, ApJ, 661, 750
van der Wel, A., Holden, B. P., Zirm, A. W., Franx, M., Rettura, A., Illingworth, G. D., & Ford, H. C. 2008, ApJ, 688, 48
van der Wel, A., & van der Marel, R. P. 2008, ApJ, 684, 260
van der Wel, A., et al. 2007, ApJ, 670, 206
van Dokkum, P. G., & Franx, M. 1996, MNRAS, 281, 985
van Dokkum, P., & van der Marel, R. 2007, ApJ, 655, 30
van Dokkum, P. G., Franx, M., Fabricant, D., Kelson, D. D., & Illingworth, G. D. 1999, ApJ, 520, L95
Vincent, R. A., & Ryden, B. S. 2005, ApJ, 623, 137
Wilman, D. J., Oemler, A. Jr., Mulchaey, J. S., McGee, S. L., Balogh, M. L., & Bower, R. G. 2009, ApJ, in press
Wuyts, S., van Dokkum, P. G., Kelson, D. D., Franx, M., & Illingworth, G. D. 2004, ApJ, 605, 677